Received: 7 February 2022 | Revised: 1 July 2022 | Accepted: 5 July 2022

DOI: 10.1111/bre.12695

Basin Research | IAS EAGE | WILEY

RESEARCH ARTICLE

Physical modelling of the interplay between salt-detached gravity gliding and spreading across complex rift topography, Santos Basin, offshore Brazil

Leonardo M. Pichel[1,2] | **Oriol Ferrer**[3,4] | **Christopher A.-L. Jackson**[1,5] | **Eduard Roca**[3,4]

[1]Basins Research Group (BRG), Department of Earth Science and Engineering, Imperial College London, London, UK

[2]Department of Earth Science, University of Bergen, Bergen, Norway

[3]Institut de Recerca UB-Geomodels, Universitat de Barcelona (UB), Barcelona, Spain

[4]Departament de Ciències de la Terra i de l'Oceà, Facultat de Ciències de la Terra, Universitat de Barcelona (UB), Barcelona, Spain

[5]School of Earth and Environmental Sciences, University of Manchester, Manchester, UK

Correspondence
Leonardo M. Pichel, Department of Earth Science, University of Bergen, Postboks 7803, 5020 Bergen, Norway.
Email: leonardo.m.pichel@uib.no

Funding information
Arthur Holmes Centenary Grant - Imperial College London; MCIN/AEI

Abstract

The Santos Basin, offshore Brazil contains a complex set of salt-tectonic structures, the origins of which are debated, that is, the Albian Gap and the São Paulo Plateau (SPP). The Albian Gap is a ca. 450 km long, 60 km wide feature characterized by a post-Albian, counter-regional rollover overlying depleted Aptian salt, and in which the Albian is largely absent. The SPP, located immediately downdip, is defined by a pre-salt structural high overlain by ca. 2.5 km thick salt. Another prominent feature is the Merluza Graben, a rift-related depocentre that underlies the southern portion of the Albian Gap and displays significant (3–4 km) base-salt relief along its main faults. Two competing hypotheses have been proposed to explain the kinematics of these provinces. One invokes post-Albian extension in the Albian Gap and kinematically-linked contraction in the SPP. The other invokes post-Albian salt expulsion in the Albian Gap and salt inflation in the SPP. Recent studies, however, suggest these processes likely alternate in time and space, contributing nearly equally to the evolution of these domains. We apply 3D physical modelling to (i) test this hypothesis; and (ii) to more generally understand how gravity gliding and spreading over three-dimensionally variable base-salt relief control regional salt tectonics. The results show a similar salt-related evolution and structural styles to those proposed in the most recent studies. They also (i) explain the origin of the ca. 25 km wide diapir precursor of the Albian Gap by early salt inflation against base-salt steps; (ii) show that normal faults with different polarities and rollover types form due to the interplay between gliding and spreading over different base-salt domains and (iii) provide a mechanism for the origin of strata encased within salt structures. This improves our understanding of the distribution and origin of salt-related structural styles in worldwide salt basins.

1 | INTRODUCTION

The Santos Basin, offshore Brazil sits centrally in several debates regarding the timing and kinematics of rifting and breakup, the temporal relationship between salt deposition and rifting, and the evolution of salt-tectonic structural styles. The main salt tectonic-related controversies revolve around the structural styles associated with the Albian Gap and São Paulo Plateau (SPP), whose geometry, origin and kinematics have been discussed for >30 years (e.g., Davison et al., 2012; Demercian et al., 1993; Jackson, Jackson, & Hudec, 2015; Jackson, Jackson, Hudec, et al., 2015; Mohriak et al., 1995; Pichel et al., 2018; Pichel, Jackson, et al., 2019; Quirk et al., 2012; Rowan et al., 2022). The Albian Gap is a remarkably large (ca. 450 km long and up to ca. 60 km wide) feature located at the transition between the updip extensional and intermediate translational salt-tectonic domains of the Santos Basin (Figure 1a,b). It is spatially and genetically associated with an equally large, 6–8 km thick, salt-detached, counter-regional rollover within post-Albian strata, and by the near-complete absence of Albian strata above a highly depleted Aptian salt layer (Figure 1b) (Guerra & Underhill, 2012; Jackson, Jackson, & Hudec, 2015; Pichel & Jackson, 2020; Rowan et al., 2022). Two competing hypotheses were originally formulated to describe its genesis and kinematics (see review by Jackson, Jackson, & Hudec, 2015; Pichel & Jackson, 2020; Rowan et al., 2022): (i) the *extensional* model, which invokes that the gap and its overlying rollover formed by >50 km of *post-Albian* gravity-driven extension accommodated by slip on a large, counter-regional listric normal fault (Cobbold et al., 1995; Demercian et al., 1993; Guerra & Underhill, 2012; Mohriak et al., 1995; Quirk et al., 2012; Rowan & Ratliff, 2012; Rowan et al., 2022); and (ii) the *expulsion* model, which argues that the Albian Gap was fully established earlier, during the Albian and that post-*Albian* deformation was driven by a basinward salt expulsion related to the differential sedimentary loading in the absence of significant lateral extension (Adam & Krézsek, 2012; Ge et al., 1997; Gemmer et al., 2004, 2005; Jackson, Jackson, Hudec, et al., 2015; Krézsek et al., 2007).

Immediately basinward of the Albian Gap is the SPP, which is characterized by thick (>2.5 km) salt capping a pre-salt structural high (the Outer High; Davison et al., 2012; Fiduk & Rowan, 2012; Gomes et al., 2009; Jackson et al., 2014; Jackson, Jackson, & Hudec, 2015; Rodriguez et al., 2019) (Figure 1). The origin and style of salt-related deformation in the SPP are linked to the Albian Gap, given they are both part of the same gravity-driven system (Jackson, Jackson, Hudec, et al., 2015). For example, *extensional* models for the Albian Gap imply that salt and supra-salt post-Albian deformation in the SPP is characterized by significant horizontal translation and regional contraction (Fiduk & Rowan, 2012; Guerra & Underhill, 2012; Quirk et al., 2012; Rowan & Ratliff, 2012; Rowan et al., 2022). Conversely, *expulsion-driven* models argue post-Albian deformation is characterized by salt inflation and growth of the SPP, but with no significant overburden translation and contraction (Ge et al., 1997; Gemmer et al., 2004; Jackson, Jackson, & Hudec, 2015; Jackson, Jackson, Hudec, et al., 2015). Recent studies argue that salt deformation in the Albian Gap and SPP is three-dimensionally more variable and complex than previously described and that a single process might not be responsible for their formation. For example, Pichel and Jackson (2020) use an extensive, depth-migrated 2D seismic dataset and balanced structural restorations to demonstrate significant lateral variability in salt-related structural style *within* the Albian Gap and to argue that both post-Albian expulsion *and* extension (ca. 30 km) played an equally important role in its evolution. This is in accordance with the magnitude of basinward translation (ca. 30 km) observed in ramp-syncline basins in the adjacent SPP (Pichel et al., 2018; Pichel, Jackson, et al., 2019). Note that this is ca. 20 km less than what would be required for an extension-dominated origin for the Albian Gap (cf. Rowan et al., 2022). Beneath the salt are numerous rift-related horsts and grabens, including the Merluza Graben (MG) (cf. Garcia et al., 2012; Magee et al., 2020) and the Outer High

Highlights

- We apply physical modelling to test hypotheses for the evolution of the controversial Albian Gap, Merluza Graben and the São Paulo Plateau, Santos Basin.
- Our 3D model evaluates the interplay between salt-detached gravity gliding and spreading over laterally variable base-salt relief.
- The Albian Gap formed by a combination of seaward salt expulsion from an Albian-age, ca. 25 km wide diapir and post-Albian overburden extension.
- The presence of a precursor, Albian-age diapir was favoured by the base-salt relief associated with the Merluza Graben where the Albian Gap is wider.
- The model also shows that different types of rollovers and fault polarity are controlled by the competition between gliding and spreading over different base-salt domains.

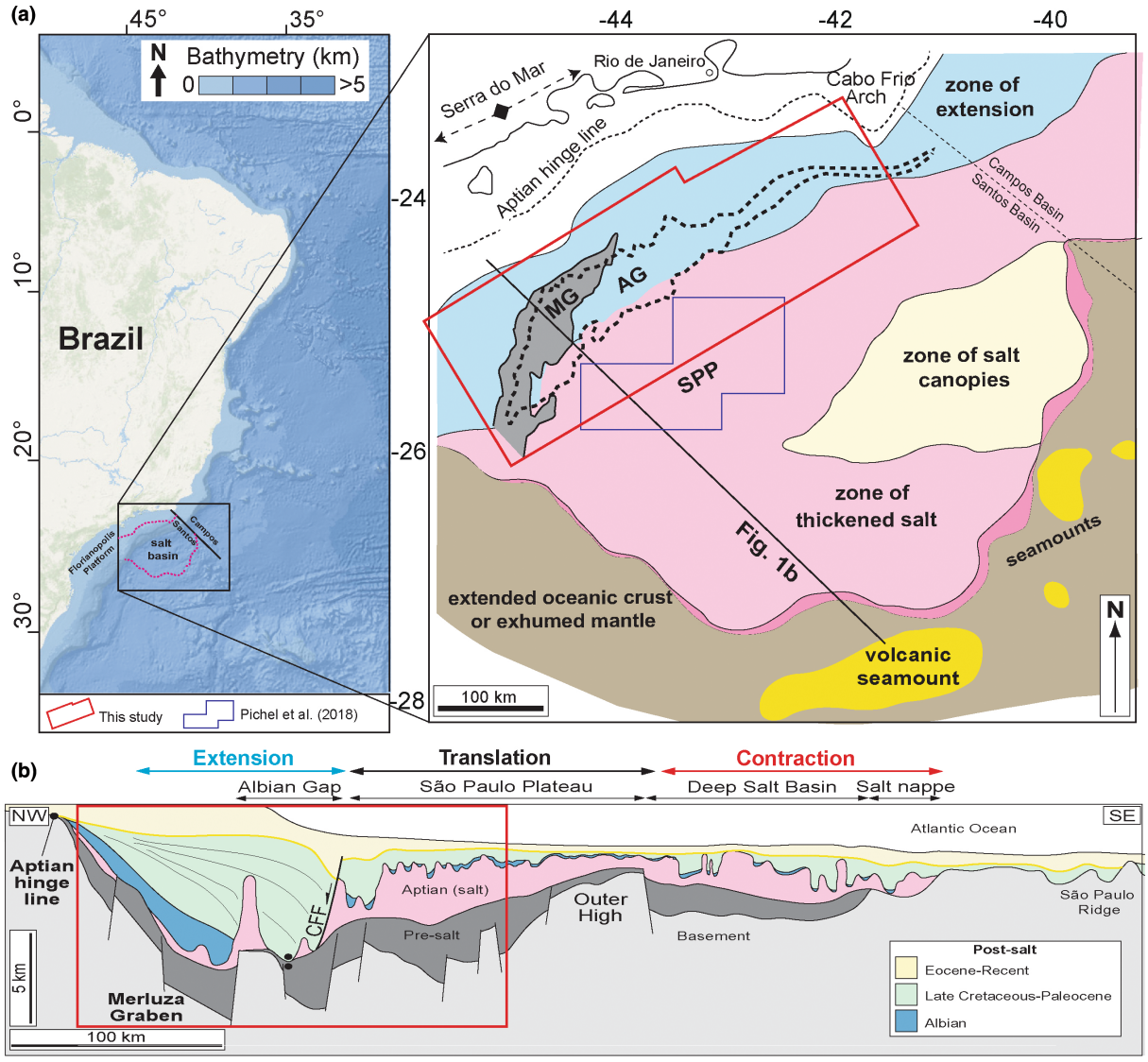

FIGURE 1 (a) Bathymetry and structural maps showing the salt-related structural domains offshore SE Brazil including the outline of the Merluza graben and Albian Gap, focus of the study and seismic datasets utilized in previous studies from Jackson, Jackson, and Hudec (2015), Pichel, Jackson, et al. (2019), Pichel et al. (2021) (adapted from Davison et al., 2012; Pichel & Jackson 2020). (b) Regional geoseismic cross-section showing the main regional salt-related structural domains offshore the Santos Basin and the area modelled in our physical experiment in red polygon (adapted from Jackson, Jackson, Hudec, et al., 2015). CFF refers to the Cabo Frio Fault bounding the Albian Gap.

(Figure 1b). The Merluza Graben is partially overlain by the Albian Gap (Figure 1a) and is characterized by large (up to 3.5–4 km) base-salt relief along its seaward limit, associated with a landward-dipping, basement-involved normal fault (Pichel et al., 2021). The presence of prominent base-salt relief in the Merluza Graben disrupts salt flow and favours the development of contractional salt structures (e.g., squeezed diapirs, salt anticlines) and ramp-syncline basins (Pichel et al., 2021) (cf. Davison et al., 2012; Mohriak et al., 2008; Quirk et al., 2012) (Figure 1a,b). Where the Albian Gap and Merluza Graben overlap, towards the southern end of the latter, there is also a clear change in the orientation (from NE to N) and the polarity of normal faults within the former as it becomes subparallel to the underlying structure (Figure 1a) (Pichel et al., 2021).

Whilst these recent, largely seismic reflection-based studies have provided advances in our understanding of salt tectonics in the Santos Basin, the kinematic and mechanical plausibility of the arising concepts have not been yet been thoroughly tested with physical models. In this paper, we use a scaled regional (i.e., representing an area 100 km long by 60 km wide) physical model of the Santos Basin to test hypotheses related to its salt-tectonic evolution, in particular, the role played by gravity gliding and spreading across three-dimensionally complex, base-salt relief.

Previous modelling studies have focused on how gliding over base-salt relief control salt-tectonic evolution; although they included sediment loading, these studies explicitly sought to minimize the contribution of margin progradation and spreading-related deformation (Dooley et al., 2017, 2018; Pichel, Finch, et al., 2019). In contrast, others have investigated the role sediment loading and spreading play in driving salt deformation, with specific emphasis on how this might control the structural style and development of counter-regional rollover structures such as the one in the Albian Gap (Ge et al., 1997; Guerra & Underhill, 2012). However, in these cases, the models neglected gliding by modelling deformation above a flat-lying salt, despite Ge et al. (1997) having base-salt steps. Our model is the first to combine gliding and spreading over base-salt relief, inspired by structures observed within (i.e., the Merluza Graben, Albian Gap and SPP) and kinematics inferred from the study of the Santos Basin (Figure 2). Given that salt-related gliding and spreading over an irregular base-salt surface is common in several other basins such as West Africa (cf. Evans & Jackson, 2020), Gulf of Mexico (cf. Hudec et al., 2020), Campos-Espirito Santo (do Amarante et al., 2021; Dooley et al., 2017), Morocco (Pichel, Finch, et al., 2019; Pichel, Huuse, et al., 2019; Tari & Jabour, 2013) and Nova Scotia (Deptuck & Kendell, 2017), our modelling results also help us understand regional salt tectonics in other salt basins.

2 | GEOLOGICAL SETTING

The Santos Basin is bound by the Cabo Frio Arch to the northeast and by the Florianopolis Platform to the southwest (Figure 1) (Garcia et al., 2012; Mohriak et al., 1995). The basin originated during the Early Cretaceous rift event that ultimately led to the opening of the South Atlantic (e.g., Heine et al., 2013; Karner & Gambôa, 2007; Kukla et al., 2018; Meisling et al., 2001; Modica & Brush, 2004; Mohriak et al., 2008). Rifting was characterized by ESE-SE extension, which formed NNE-to-NE-oriented grabens and half-grabens filled by Barremian, syn-rift, fluvial-lacustrine deposits, overlain by an early-to-middle Aptian, carbonate-dominated sag (i.e., early post-rift) sequence (Davison et al., 2012; Meisling et al., 2001). Regional fault activity decreased during the early Aptian and, by the Late-Aptian a ca. 2.5 km thick (on average) salt succession had been deposited (Davison et al., 2012; Garcia et al., 2012; Pichel & Jackson, 2020). Salt deposition and distribution were controlled by relief inherited from the preceding rift, resulting in spatial variations in the original thickness and composition of the salt (Davison et al., 2012; Garcia et al., 2012; Rodriguez et al., 2019). In pre-salt lows such as the Merluza Graben and the Deep Salt Basin, salt was up to 3.5–4 km thick (Figure 1b) (Garcia et al., 2012; Lebit et al., 2019). Conversely, on pre-salt highs such as the Outer High underlying the SPP (Figure 1b), salt was only ca. 1–2 km thick (Davison et al., 2012; Garcia et al., 2012; Rodriguez et al., 2019).

During the early Albian, the Santos Basin became fully marine due to continental breakup, the emplacement of oceanic crust, and related thermally induced post-rift subsidence (Quirk et al., 2012). During the late Albian, the basin tilted south-eastward towards the developing spreading centre, inducing gravity gliding of the salt and its overburden. Salt-related deformation produced numerous thin-skinned, predominantly basinward-dipping, salt-detached normal faults that dismembered the Albian carbonate layer into rafts in the updip extensional domain (zone of extension, Figure 1) (Cobbold et al., 1995; Demercian et al., 1993; Guerra &

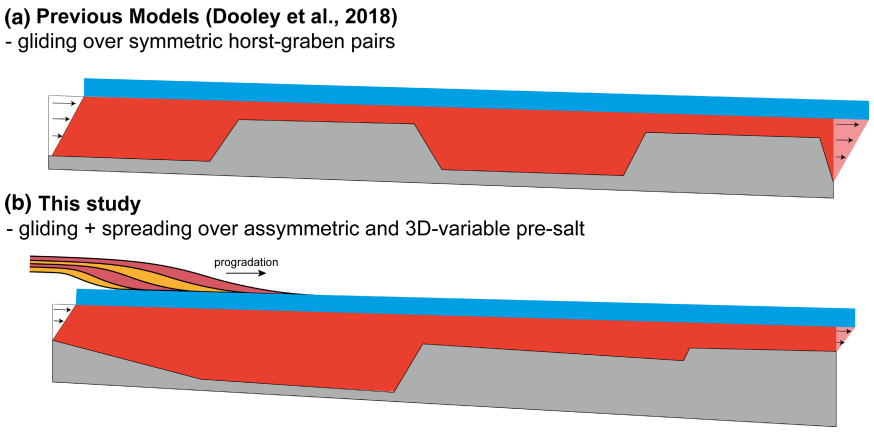

FIGURE 2 (a) Synthetic diagram of previous modelling scenarios (Dooley et al., 2017, 2018) investigating the effects of base-salt topography on salt flow associated with basinward tilting, gravity gliding and symmetric base-salt structures. (b) Synthetic diagram illustrating our modelling scenario where we test the interplay of gliding and spreading over asymmetric base-salt structures characterized by half-grabens and landward-dipping normal faults as observed in the Santos Basin.

Underhill, 2012; Quirk et al., 2012). Post-Albian sedimentation was characterized by margin-scale clastic progradation, with sediments derived from the uplifting of the Serra do Mar Mountain range (Figure 1a) (Modica & Brush, 2004). Due to the margin progradation, deformation gradually migrated downdip into the Albian Gap and onto the SPP (Figure 1) (Jackson, Jackson, & Hudec, 2015; Pichel & Jackson, 2020; Quirk et al., 2012). Post-Albian salt tectonics was characterized by the basinward expulsion of salt from the Albian Gap, and the development of a hybrid, extensional-expulsion counter-regional rollover (Pichel & Jackson 2020); this was kinematically balanced by up to ca. 30 km of overburden translation above inflated salt in the SPP (Pichel et al., 2018; Pichel, Jackson, et al., 2019). This interpretation has been recently challenged by Rowan et al. (2022) who argues a dominant, >50 km of post-Albian extension in the Albian Gap and equivalent, ca. 50 km of translation and shortening downdip in the SPP. There, salt deformation was influenced by the rift-related base-salt relief and salt thickness variability in the Outer High, which resulted in salt flux variations and broadly coeval extension, contraction, load-driven diapirism and development of ramp-syncline basins (Pichel et al., 2018; Pichel, Jackson, et al., 2019). The Albian Gap, Merluza Graben and the Deep Salt Basin were likely also influenced by base-salt relief due to the complex rifting and break-up history of the basin (Figure 1b) (cf. Davison et al., 2012; Garcia et al., 2012; cf. Pichel & Jackson, 2020; Pichel et al., 2021).

3 | ANALOGUE MODELLING

3.1 | Experimental setup

Our model simulates the salt-tectonic evolution of the proximal portion of the southern Santos Basin, comprising its updip salt pinch-out and three main structural provinces: the sub-salt Merluza Graben, and the supra-salt Albian Gap and SPP (Figures 3 and 4). The first is built-in the model setup and the other two arise as a function of salt-related deformation. This represents a three-dimensionally complex structural setting, in which the pre-salt relief related to the Merluza Graben and adjacent base-salt steps vary along-strike in terms of their steepness and orientation, resulting in differences in salt basin geometry and salt thickness (Figures 4–6). As we show below, this produces spatial and temporal variations in the contributions and styles of gravity-driven gliding and spreading, resulting in complex and multiphase salt tectonics (Figures 5 and 6). We thus divide the model into North and South Domains, in which the base-salt structures are oriented orthogonal and oblique, respectively, to the main direction of gravity-driven tectonic transport; and a central area where these domains intersect (Figure 4). The 3D model thus comprises three different structural settings based on the variable base-salt configuration. We also sub-divide the Merluza Graben into three different portions: Updip, Central and Merluza Fault for simplicity in the model descriptions.

Physical modelling was undertaken at the Geomodels Analogue Modelling Laboratory (Universitat de Barcelona) in a deformation rig that was 120 cm long and 70 cm wide (Figure 4a). Two fixed lateral glass walls and two metal plates confined the analogue materials during the model run. Dry silica sand was used to build the sub-salt topography, and a mixture of silica sand and clay was used locally to sculpt a steeper dip for the sub-salt faults. We modelled two major landward-dipping, sub-salt steps that change orientation along strike (from orthogonal to oblique to the tectonic transport direction) (Figure 4a). These steps are equivalent to major sub-salt faults observed in the basin, the first is the Merluza Fault and the second represents a set of closely spaced faults at the transition to the SPP (Figure 1b). The orientation, geometry and width of the sub-salt grabens and highs are scaled and equivalent to the ones observed in nature (compare Figures 3 and 4). The throw associated with the sub-salt faults are kept constant, being an average of the throw along their central portion observed in nature, for model simplification purposes. The baseplate was tilted 4° and the polymer was emplaced above the pre-salt topography. After 48 h, when the polymer had settled, a 5 mm-thick, pre-kinematic layer of blue sand was manually poured above the entire model and levelled with a scraper (Figure 4b). This initial tilting was implemented to create the rift-related base-salt relief measured along the pre-salt tilted fault-blocks observed in the study-area, that is, the tilting did not trigger deformation as both the salt and pre-kinematic layer were horizontal. Deformation was only triggered in the next stage by tilting of the baseplate a further 2° basinward (driving gravity gliding) and by adding a wedge of 4 mm thick blue sand (driving gravity spreading) (Figure 4c). The post-salt (post-rift) tilt modelled is consistent with what is observed in regional seismic profiles in the study-area (Figure 1b) (Davison et al., 2012; Pichel et al., 2021; Rodriguez et al., 2019). It is also consistent with previous physical modelling studies of regional salt tectonics and is interpreted to be caused by post-rift thermal subsidence (cf. Brun & Fort, 2011; Dooley et al., 2007; Jackson & Hudec, 2017).

Syn-kinematic prograding wedges of white and coloured (red and yellow) dry silica sand were poured onto the experiment and then levelled every 2 h. This

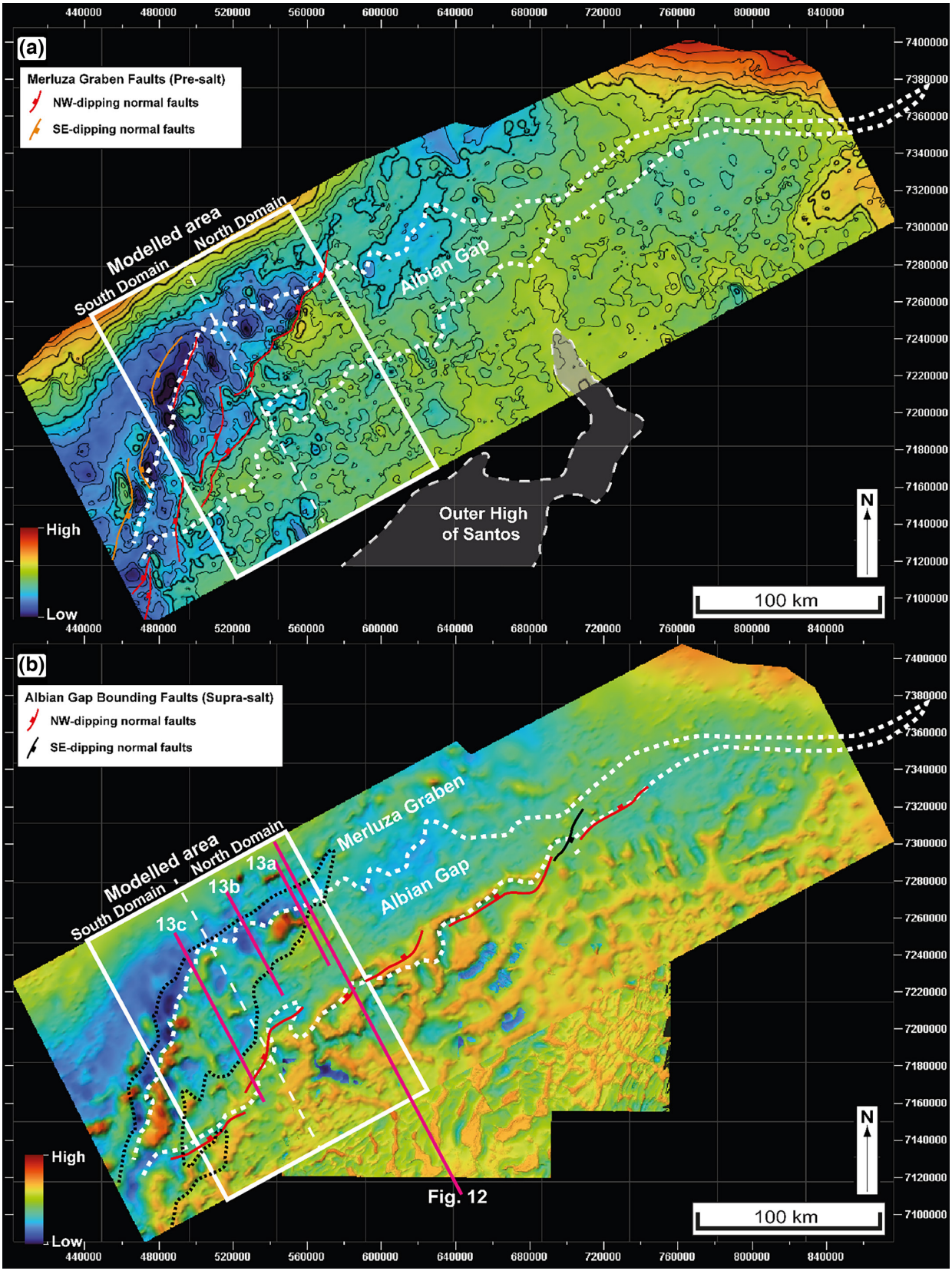

FIGURE 3 (a) Base-salt and (b) top-salt maps adapted from Pichel et al. (2021) showing the outline of the Merluza graben, a major and complex NNE-NE-oriented base-salt structural low, and the overlying Albian Gap, a 450 km wide and 30–65 km wide structure characterized by a structurally lower top-salt bounded basinward by large landward-dipping normal faults and inflated, wide salt diapirs in the Sao Paulo Plateau. The Sao Paulo Plateau is characterized by predominantly NE-NNE-oriented salt structures that formed over a prominent base-salt structural high, the outer high of Santos.

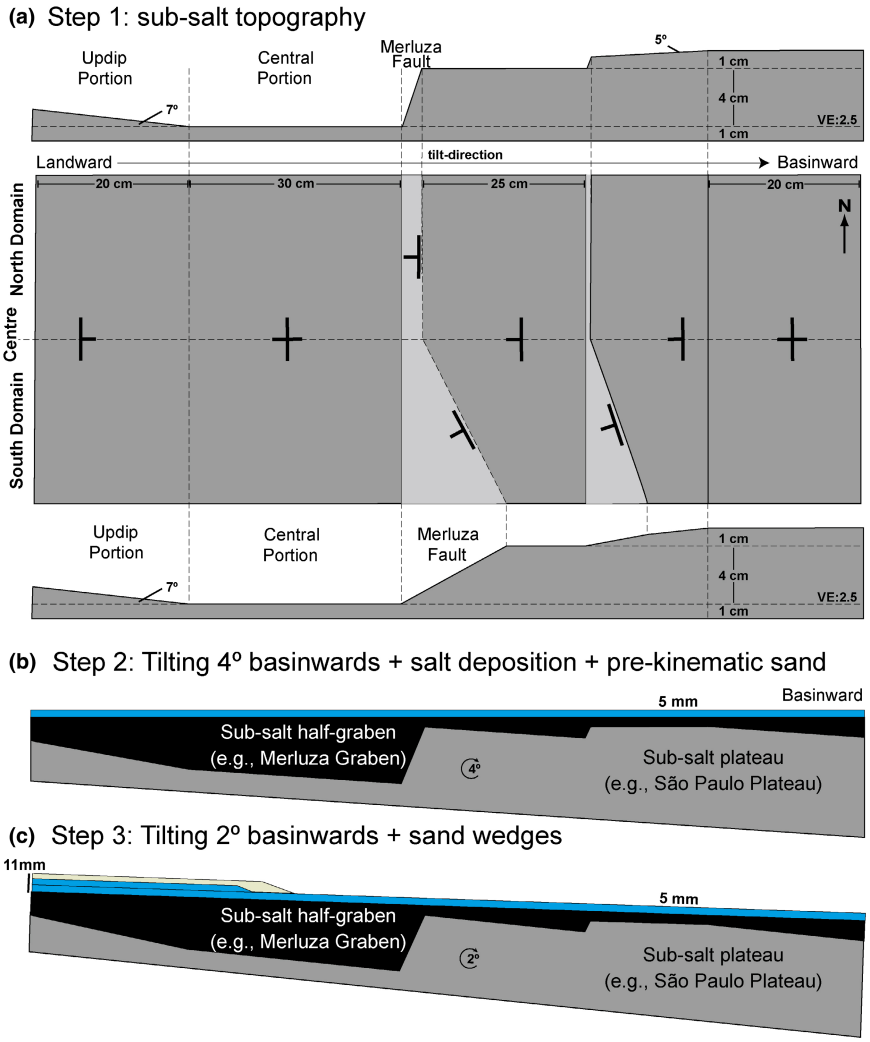

FIGURE 4 Synthetic diagram illustrating the pre-salt model setup in (a) map-view and cross-section with two different base-salt domains, the north and south domains where base-salt topography is oriented orthogonally and oblique to tectonic transport, respectively. In (b), cross-section illustrating the initial salt thickness variability across base-salt structures and pre-kinematic post-salt interval in blue. In (c), cross-section showing the onset of salt deformation driven by 2° tilting of the model and differential loading by sand wedges.

time-interval was chosen because it: (i) stopped the unrealistic breakout of salt and the emplacement of allochthonous bodies (e.g., sheets), which are not observed in or downdip of the Merluza Graben; yet (ii) permitted the growth of salt diapirs, which are common across the study area. As a result, our models are kinematically and geometrically consistent with nature. Prior to the deposition of each syn-kinematic wedge, the baseboard was tilted back 2°. The regional datum was progressively raised 1 mm before the deposition of each sand wedge. The roof of the main salt structures elevated above the regional datum during the experiment were systematically vacuumed to simulate erosion. After the deposition of each syn-kinematic wedge, the baseboard was again tilted 2° basinward to restart gravitational gliding. A trench of sand and polymer was gradually removed at the basinward metal plate to create an open-toe system. At the end of the model run, we covered the experiment with a fine-grained, post-kinematic, dry silica sand to preserve the final topography and inhibit further polymer flow. Finally, we sectioned the model into 200 3 mm-thick vertical slices.

3.2 | Materials

A well-sorted and rounded dry silica sand (white and coloured) with an average grain size of 200 μm was used to simulate brittle rocks of the upper continental crust (pre-salt and overburden in our natural analogue). It is generally accepted that dry silica sand obeys a Mohr-Coulomb failure criterion at laboratory strain rates (Horsfield, 1977; Hubbert, 1951). The mechanical properties of this sand were measured by Ferrer et al. (2017), who demonstrated an angle of internal friction ($ø$) of 34.6°, a coefficient of internal friction (φ) of 0.69, a bulk density of 1500 kg m^{-3}, and a low apparent cohesive strength of 55 Pa. A transparent, high-viscosity silicone polymer (polydimethylsiloxane or PDMS) was used to model rock salt (referred in the text as "salt" for simplicity). PDMS is a near-Newtonian viscous fluid that, at laboratory strain rates, has a low yield strength, similar to the behaviour of natural salt (e.g., Dell'Ertole & Schellart, 2013; Weijermars & Schmeling, 1986). At room temperature, PDMS has a density of 974 kg m^{-3} and a viscosity of 1.6×10^{-4} Pa s when deformed at a

laboratory strain rate of 1.83×10^{-4} cm s^{-1} (Dell'Ertole & Schellart, 2013). Table 1 summarizes the scaling parameters of the experiments as well as the mechanical properties of the modelling materials.

3.3 | Model analysis

Computer-controlled high-resolution digital cameras took overhead and oblique, time-lapsed photographs during the experiment to document the model kinematics. In addition, we also took photographs of specific structures to aid our analysis of the model results. We used overhead time-lapse photographs and digital image correlation (DIC) to quantify particle displacements and strain (Adam et al., 2005). The final sections of the model were also documented by high-resolution photographs to analyse the spatial variability of the arising salt-tectonic structures.

4 | RESULTS

We first show the map-view evolution of the model using overhead time-lapse photography (Figures 5 and 6) and DIC data (Figures 7 and 8). We then describe multiple cross-sections through different domains (South and North Domains) of the model to highlight the arising salt-tectonic structural styles, before comparing them with natural examples from the Santos Basin. We refer to the sub- and supra-salt main domains and features using the same name as the nature prototype (i.e., Santos Basin) for simplicity.

4.1 | Overhead evolution

The earliest stages of the model evolution correspond to deposition of the first two sedimentary wedges simulating Albian strata and initial seaward tilting of the model

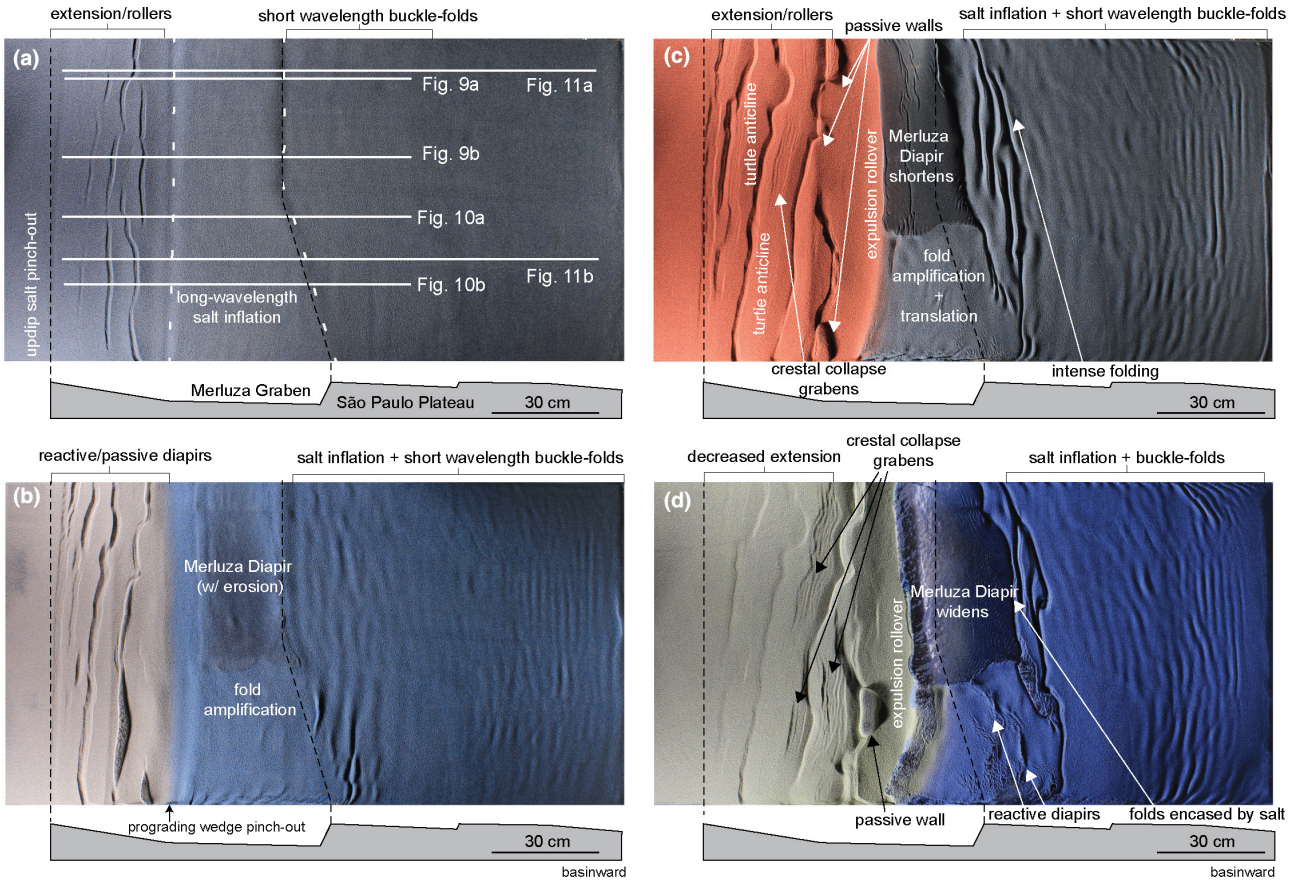

FIGURE 5 From (a–d), map-view snapshots of the early stages of the physical experiments when post-salt sediments prograde up to the largest landward-dipping sub-salt fault, equivalent to the Merluza fault. Deformation is focused within the associated graben, that is, the Merluza graben and is characterized by updip extension, and downdip salt inflation against the Merluza fault whilst further downdip there is salt-cored buckle folding. Early-stage erosion is simulated by removing the sediments above largest diapir formed above the graben, which allows the diapir to reach the surface and advance and widen beyond the graben onto the adjacent base-salt plateau. White lines in (a) indicate the cross-sections shown in Figures 9–11. Prograding sediment wedges pinch-out is marked by the change of colours in each figure as indicated in (b).

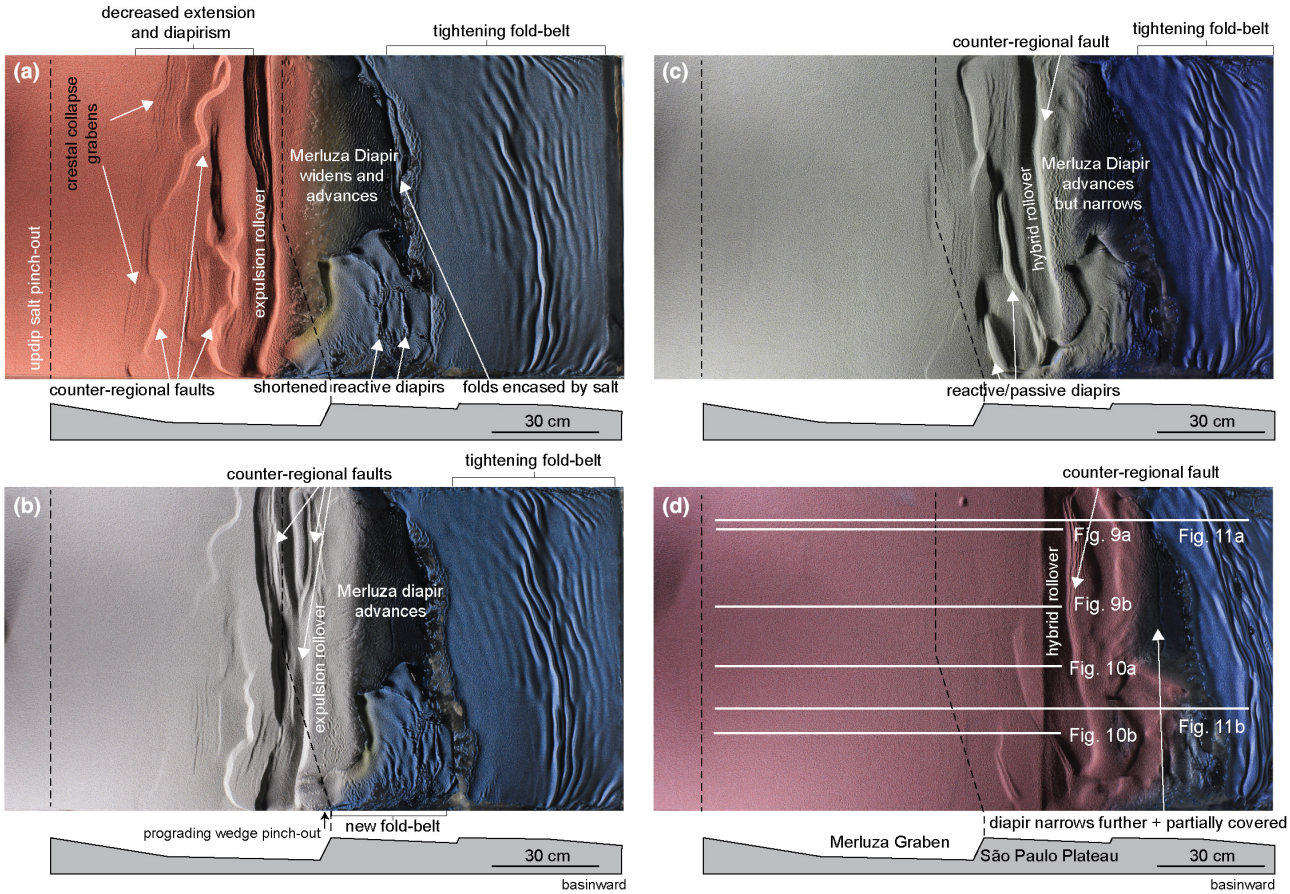

FIGURE 6 From (a–d), map-view snapshots of the late stages of the physical experiments when post-salt sediments prograde beyond the largest sub-salt half-graben, the Merluza graben and onto the downdip sub-salt plateau. Deformation progresses and advances gradually basinward onto the sub-salt plateau as post-salt sediments prograde. The diapir formed previously advances further basinward, moving completely over the sub-salt plateau whilst extension and load-driven rollovers and turtle structures form updip against the Merluza fault. The area of previously inflated salt moves laterally and extends, forming reactive diapirs in the south as it moves beyond the Merluza fault. White lines in (d) indicate the cross-sections shown in Figures 9–11. Prograding sediment wedges pinch-out is marked by the change of colours in each figure as indicated in (b).

(Figures 4c and 5a,b). At this time, deformation is focused within the large sub-salt half-graben that represents the Merluza Graben (Figures 5a, 7a and 8a). Broadly symmetric and linear grabens that are cored by reactive diapirs and salt rollers and bound by normal faults that develop in the updip portion of the graben. At its central and Merluza Fault portions, the Merluza Graben is overlain by a wide zone of inflated salt and relatively gentle folded overburden (Figures 5a and 8a). This zone of inflation follows the sub-salt trend, thus being wider and oblique to gravity-driven transport in the south. Minor, short-wavelength buckle-folds form further downdip of the half-graben, above the adjacent sub-salt plateau that represents the SPP (Figures 5a and 8a).

Earlier-formed structures are amplified during deposition of the second sedimentary wedge, which represents Upper Albian strata (Figures 4c and 5b). Updip extension is preferentially accommodated along basinward-dipping normal faults, with salt reaching the surface at the core of early formed grabens, forming linear reactive-passive salt walls. The ongoing basinward evacuation and inflation of salt above the Merluza Graben results in amplification of the previous structures, that is, the salt plateau and gentle overburden folds further downdip (Figure 5b). To the north, where the Merluza Graben is narrower (30 cm), there is greater salt inflation and overburden uplift than in the south where: (i) the graben is wider; and (ii) its associated base-salt step trends oblique rather than normal to the overall direction of transport (Figures 4a and 5b). During this stage, overburden erosion results in the development of a 25–30 cm wide salt diapir (herein referred to as the Merluza Diapir) that reaches the model surface in the north of graben (Figure 5b). Further downdip, over the SPP, there is widespread salt inflation and overburden buckle-folding (Figure 5b).

In the next stage, equivalent to early post-Albian times, continued progradation results in additional updip extension and basinward translation of supra-salt structures,

TABLE 1 Scaling parameters used in the experimental programme

Parameter	Experiment	Nature	Model ratio
Thickness			
Pre-kinematic overburden	0.5 cm	500 m	10^{-5}
Syn-kinematic overburden	0–6 cm	0–600 m	10^{-5}
Salt/polymer[a]	0–4.5 cm	0–4500 m	10^{-5}
Density			
Overburden	1500 kg m^{-3}	2700 kg m^{-3}	0.55
Salt/polymer	972 kg m^{-3}	2200 kg m^{-3}	0.44
Density contrast	528	500	1.05
Ductile layer viscosity	1.6×10^{-4} Pa s	10^{-18}–10^{-19} Pa s	1.6×10^{-14}–1.6×10^{-15}
Overburden coefficient friction	0.7	0.8	0.87
Gravity acceleration	9.81 m s^{-2}	9.81 m s^{-2}	1

[a]Thickness at the beginning of the experiment.

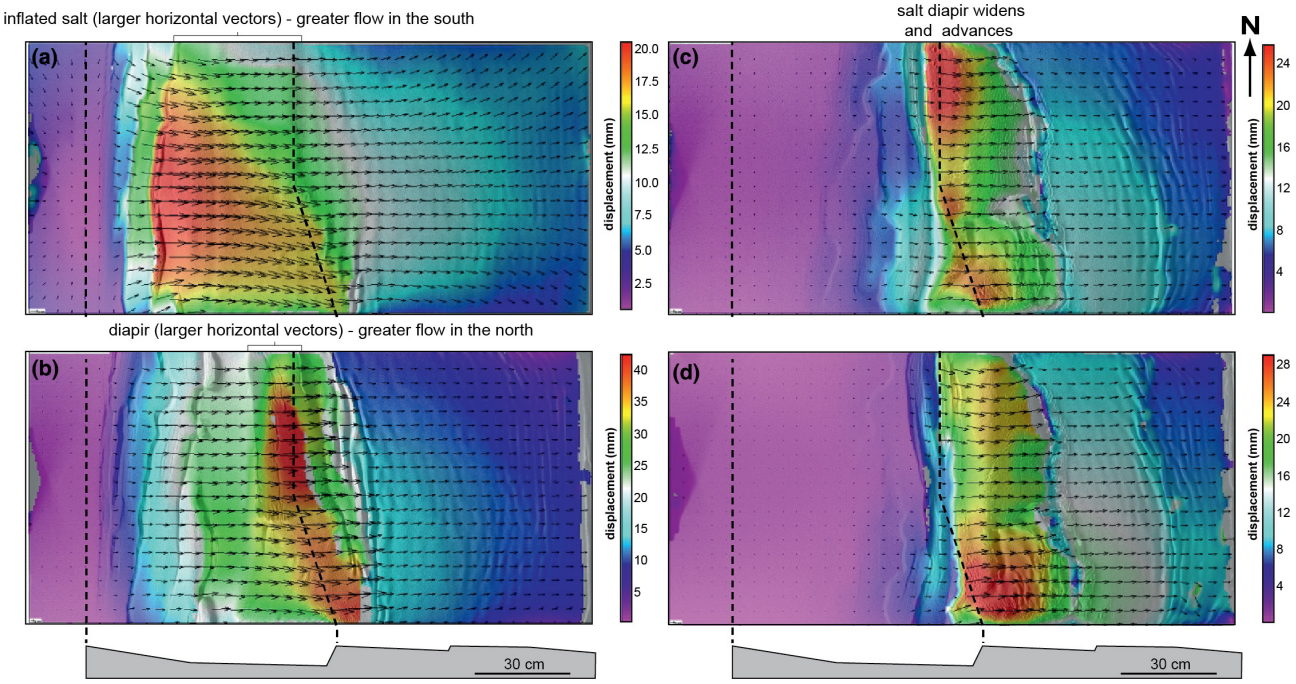

FIGURE 7 2D DIC overhead imagery showing displacement (vectors) and the associated deformation at key time-steps throughout model evolution. Colours indicate the magnitude (mm) of horizontal deformation and the arrows are vectors showing the magnitude and direction of particles movement for a specific progradational wedge. (a,b) Early stages of model evolution when progradation and deformation are concentrated updip and within the Merluza graben being characterized by updip extension and significant salt inflation against its bounding fault. Note diapir breakthrough at the northern part of the model where both the sub-salt Merluza graben and the zone of salt inflation are narrower. (c) Intermediate stage when progradation reaches the Merluza fault and the previous inflated salt and large diapir translate beyond it, above the base-salt plateau. (d) Late stage when progradation reaches the sub-salt plateau and the bulk of deformation migrates beyond the Merluza graben, being focused over the previously inflated salt. Note divergence of vectors in the Centre and southern portion of the model where the sub-salt structure is oblique to direction of tectonic transport. Note also larger vectors demonstrating greater magnitude of lateral movement where the inflated salt reaches the surface and form diapirs.

with new normal faults and extensional turtle anticlines developing in the updip portion of the Merluza Graben (Figure 5c). Some of the earlier formed walls are buried, while new ones form further downdip, but still within the graben (Figure 5c). In the north domain, the wide (ca. 22 cm) diapir inflates further and starts to translate basinward,

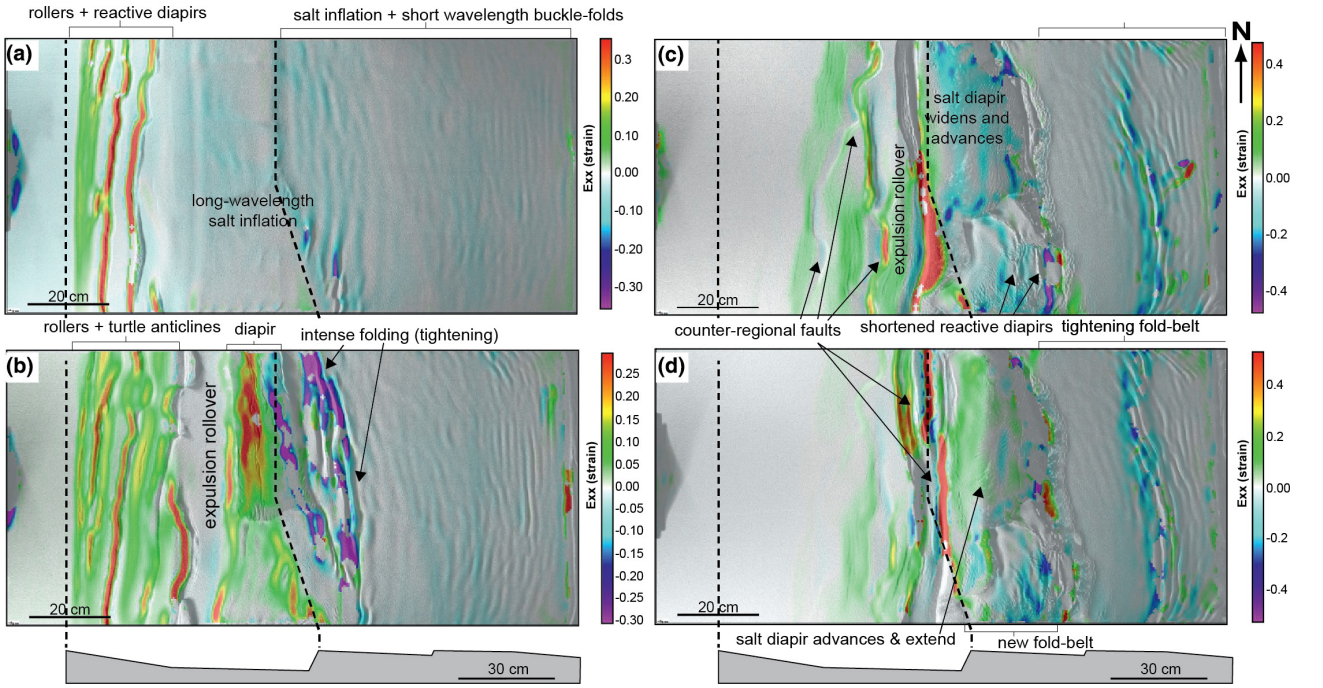

FIGURE 8 DIC overhead imagery showing horizontal strain: Positive values (warmer colours) denote extension and negative values (cold colours) indicate shortening throughout model evolution, at the same time-steps of Figure 7. (a) Initial stage showing that the bulk of deformation is focused in the updip portion of the model in the form of linear extensional structures updip of the Merluza graben and inflated salt with salt-cored folds above and adjacent to the Merluza graben. (b) Early stage when a wide salt diapir forms above the northern portion of the Merluza graben and accommodates most of the deformation and salt inflation within the area. This diapir and the laterally equivalent inflated salt to the south are affected by outer-arc extension above their crest, which is located updip of the Merluza fault whilst being shortened and developing folds at its downdip portion above and adjacent to the Merluza fault. Intermediate stage, (c) the diapir translates basinward above base-salt relief whilst being shortened at the toe-of-slope as it becomes covered by sediments whilst previous extensional structures located in the south are squeezed. At late stages (d), extension migrates basinward, being concentrated at the downdip portion of the Merluza graben. The large diapir formed above the Merluza graben widens and extends underneath the upper-slope as most of its salt is able to translated basinward beyond the Merluza fault. Shortening occurs to the south of the diapir in the form of squeezing of smaller, previously extensional diapirs and basinward by buckle-folding against the downdip base-salt step.

beyond the Merluza Fault (Figures 5c, 7b and 8b). The updip side of the Merluza Diapir, the one located above the sub-salt graben, is further inflated and bound by an expulsion rollover that extends along the entire strike-length of the model (Figures 5c and 8b). Further downdip, over the SPP, new salt-cored buckle folds form whilst earlier-formed folds are tightened (Figures 5c and 8b).

In the next stage, as the margin progrades, the most proximal salt structures become dormant as most of the salt is expelled downdip, eventually welding in the updip portion of Merluza Graben. Further basinward, extension continues within the Merluza Graben, with further growth of reactive and passive diapirs, the latter of which starts widening (Figure 5d). The post-Albian sediments and the associated expulsion rollover reach the Merluza Fault (Figure 5d). At this stage, the post-salt sediments completely fill the Merluza Graben (as observed by the first green post-salt wedge terminating at the same height as and against the crest of the Merluza Fault, Figures 9–11) and expel most of its salt basinward. The Merluza Diapir inflates and widens, from ca. 20 to ca. 34 cm. The diapir also translates almost entirely beyond the Merluza Fault in the northern portion of the model (Figure 5d). In the southern portion, where the inflated salt remained largely covered by Albian-equivalent strata, reactive and passive diapirs form in response to ongoing overburden extension and dismembering of their roofs (Figure 5d).

In the following stage (Figures 6a, 7c and 8c), as sediments prograde beyond the Merluza Graben, there is little deformation in its updip portion where the salt has been mostly welded. Extension migrates basinward and is primarily accommodated by counter-regional (i.e., landward-dipping) normal faults over the central portion of the Merluza Graben (Figures 6a and 8c). The expulsion rollover formed at the updip edge of the Merluza Diapir is faulted and associated with counter-regional normal faults (Figures 6a and 8c). The Merluza Diapir widens (reaching up to ca. 38 cm) and translates further basinward, merging laterally with passive salt walls to the south, whilst developing new low-amplitude folds above and ahead of it

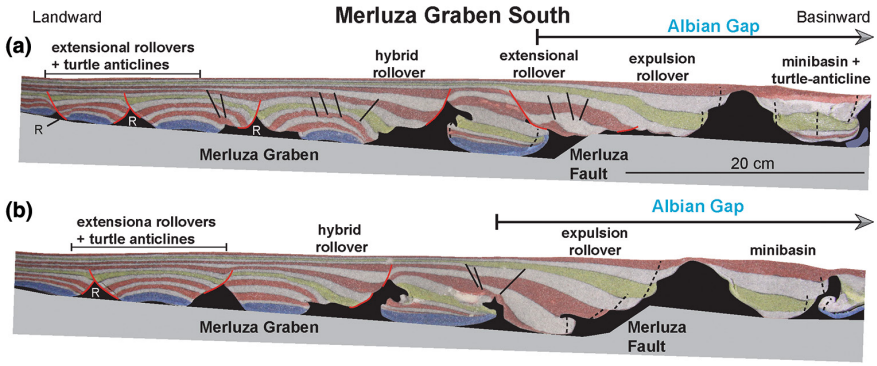

FIGURE 9 Physical model detailed sections from the north domain. Deformation is characterized by updip salt rollers (R), and extensional turtle anticlines passing downdip to extensional and/or hybrid rollovers and more complex diapirs near the Merluza fault. Further downdip, deformation above the sub-salt plateau is characterized by more complex structures such as salt rollers, extensional and expulsion rollovers, turtle-anticlines and tall diapirs bounded by highly upturned minibasin strata. Note the absence of blue material over the Merluza Fault and the sub-salt plateau defining the Albian Gap. Location of profiles shown in overhead Figures 5a and 6d.

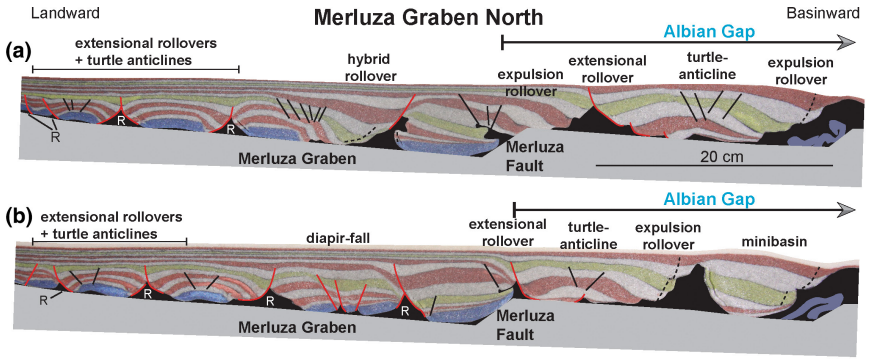

FIGURE 10 Physical model detailed sections from the south domain. Similar to the north domain, updip deformation is characterized by salt rollers and turtle anticlines updip passing downdip to extensional and/or hybrid rollovers and more complex diapirs near the Merluza fault. A large basinward-dipping rollover occurs near and above the Merluza fault where the blue post-salt section is absent. Larger diapirs occur above and/or near the Merluza fault being bounded by upturned strata, minibasins and/or turtle anticlines. Note the absence of blue material over the sub-salt plateau defining the Albian Gap. Blue, Albian-equivalent strata are encased within salt diapirs in the São Paulo plateau. Location of profiles shown in overhead Figures 5a and 6d.

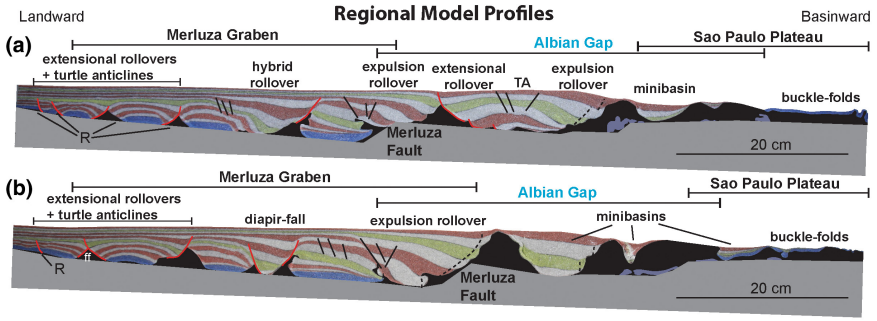

FIGURE 11 Regional model sections from (a) north domain, and (b) south domain illustrating the main salt-related structural styles of both domains and their relationship with the updip Merluza graben, the Albian Gap, where the first post-salt interval is absent, and the inflated salt and associated fold-belt formed in the downdip end of the model, over the Sao Paulo Plateau. Location of profiles shown in overhead Figures 5a and 6d.

(Figures 6a and 8c). The reactive diapirs formed above the inflated salt in the south are squeezed as they approach the downdip base-salt step (Figures 6a and 8c).

The style and evolution of salt-tectonics in this stage are similar to the preceding one, being characterized by margin progradation and the basinward migration of extension

(Figures 6b, 7d and 8d). This results in amplification and advance of counter-regional faults and the downdip expulsion rollover, as well as the complete burial of the most proximal salt structures (Figure 6b). The Merluza Diapir continues to widen (to a total width of up to ca. 40 cm), advance basinward and expand laterally by coalescing with passive salt walls in the south, while a new foldbelt forms in between them where the salt remained covered by the Albian (Figures 6b and 8d). Significant along-diapir variability is observed at this stage. For example, the Merluza Diapir is shortened in the south where it remained partially covered by post-salt sediments, whilst it widens in the north where it had reached the model's surface and thus could translate faster (Figures 6b, 7d and 8d). The distal foldbelt is tightened as salt flow is partially buttressed over base-salt steps and by the gradual basinward-thinning of salt over SPP (Figures 6b, 7d and 8d).

In the next stage, the structures within the Merluza Graben become largely dormant due to continuous basinward salt evacuation onto the SPP and consequent depletion within the half-graben (Figure 6c). Updip deformation in the northern portion of the Merluza Graben is characterized by the development of counter-regional normal faults and basinward-dipping extensional rollovers and/or turtle anticlines, most of which are associated with crestal collapse grabens formed due to outer-arc extension (Figure 6c). In contrast, the southern portion of the Merluza graben contains 10–20 cm long, reactive-passive walls that are bound by large counter-regional faults formed during the previous stage (Figure 6b-c). The expulsion rollover also becomes bound by a large counter-regional normal fault at its basinward edge and is thus classified as a hybrid rollover formed by a combination of salt expulsion and overburden extension (Figure 6b–c) (see Pichel & Jackson, 2020). The adjacent Merluza Diapir now starts to narrow (down to ca. 30 cm) and rise while still translating seaward (Figure 6c).

At the last stage, progradation results in complete burial of all salt structures updip and within the Merluza Graben, and nearly complete burial of structures in the updip portion of the SPP (Figure 6d). Extension is thus localized along the largest counter-regional fault and its overlying rollover, adjacent to the inflated salt over the sub-salt plateau (Figure 6d).

4.2 | Cross-sectional architecture and 3D variability

This multiphase and complex structural evolution described above is also recorded by the cross-sectional geometry of salt and post-salt structures (Figures 9–11). Due to the lateral variability of the base-salt relief in our model, we present and describe regional (Figure 11) and detailed cross-sections for both its southern (Figure 9) and northern (Figure 10) domains representing the Merluza Graben, and the Albian Gap and SPP.

4.2.1 | Merluza graben

The cross-sections demonstrate a transition from predominantly extensional deformation at the updip portion of the sub-salt half-graben, equivalent to the Merluza Graben, to a more complex, multiphase deformation against its bounding landward-dipping fault, equivalent to the Merluza Fault (Figures 9–11). In the northern and southern domains, updip extension is associated with the development of listric normal faults, which are dominantly basinward-dipping updip of the half-graben and landward-dipping within the graben itself. These faults are flanked by salt rollers, extensional rollovers, and/or turtle anticlines (Figures 9–11). The Albian succession form a series of dismembered rafts that are spaced 2–6 cm (blue in Figures 1b, 9–11). Salt rollers associated with extensional turtles and collapsed diapirs are also observed in the updip and central portions of the Merluza Graben (Figures 9, 10 and 11b).

Salt structures developed downdip within the Merluza Graben (central and Merluza Fault portions) are more variable. They are flanked by upturned and thinned, near-diapir strata (*axial-traces in dashed black lines*, Figures 9–11), characteristic of halokinetic sequences, which indicate an early phase of salt expulsion and load-driven diapirism. This is followed by late extension and diapir collapse, expressed by the development of large, landward-dipping normal faults and hybrid rollovers (Figures 9a, 10 and 11a). These structures are also flanked by small, ca. 1 cm-wide salt wings and/or inflated diapir bulbs, suggesting a degree of shortening and minor salt extrusion prior to extension (Figures 9 and 10). Further downdip, above the Merluza Fault, there is significant along-strike structural variability. To the north, adjacent to (*dashed black lines*, Figures 9a and 11a) or above (Figure 9b) the Merluza Fault, are upturned and thinned Albian strata, whereas in the south the Albian forms broadly tabular rafts that typically terminate 5–8 cm updip of the fault (Figures 10 and 11b). Diapirs overlying or just downdip of the sub-salt fault display complex cross-sectional geometries, being defined by 2–3 cm wide, landward-verging salt tongues that are near-parallel to the post-Albian strata (Figures 9–11). These tongues form due to salt flowing landward into topographic lows within the rollovers. The geometry of post-Albian strata above the Merluza Fault can vary from near-diapir upturn

(Figures 9a,b, 10a and 11a), to large expulsion rollovers above depleted salt or adjacent to large diapirs (Figures 9a, 10 and 11).

4.2.2 | Albian Gap and SPP

The area immediately downdip of the Merluza Graben corresponds to a 25 cm wide, sub-salt high that is characterized by the complete absence of blue sand (i.e., equivalent to Albian strata). This gap, which we interpret as equivalent to the Albian Gap (cf., Jackson, Jackson, Hudec, et al., 2015; Mohriak et al., 1995), extends further landward onto the Merluza Graben, and basinward onto the SPP, varying in width from 30 to 40 cm in the southern domain to 40–50 cm in the northern domain (Figures 9–11). The structure is characterized by welded to depleted salt that is overlain by post-Albian rollovers and turtle anticlines (Figures 9–11). It also contains less prominent, post-Albian, bowl-shaped minibasins with significant near-diapir upturned strata in their most distal portions (Figure 11).

The overhead views described earlier show that the hybrid rollovers and turtle anticlines are formed by a combination of overburden extension and load-driven salt expulsion into adjacent diapirs (Figures 9–11). These two processes and their resultant structures are spatially and temporally related, occurring at different times and in different places as the post-Albian sediments prograde. Extension is accommodated by the formation of basinward-dipping listric normal faults (*red*) at the flank of and above diapirs along the updip portion of the Albian Gap, on the footwall of the Merluza Fault (Figures 9 and 11a). Load-driven salt expulsion and diapirism are recorded by sigmoidal, rollover-style stratal geometries that are associated with sediment wedges that thicken basinward, before thinning and upturning against large (3–4 cm tall and 5–6 cm wide) diapirs to form halokinetic sequences (cf., Giles & Rowan, 2012; Pichel & Jackson, 2020) (Figures 9–11). Extensional diapirs are narrow, asymmetric, triangular and have relatively planar flanks, typical of rollers, whereas the ones associated with load-driven processes are broader and have more irregular, stepped flanks (Figures 9 and 10). In the northern domain, where the Albian Gap is wider, the post-Albian diapir geometries are more variable and present more evidence for extension, that is, normal faulting (Figures 9 and 11a). In the southern domain, there is little visible extension and turtle geometries are less prevalent, although the diapirs are generally larger (ca. 1 cm taller and 3–5 cm wider, Figures 10 and 11a).

Further basinward, over the next base-salt high defining the SPP, there are broad (ca. 4–10 cm wide) diapirs that pass basinward onto salt-cored buckle-folds (Figure 11). The diapirs commonly reach the surface or are covered by very thin (<1 cm) post-Albian equivalent strata, and are surrounded by 1–3 cm thick, post-Albian minibasins. Some of these diapirs present also encased and highly deformed Albian strata within the salt (Figures 9–11). The post-salt buckle-folds comprise broadly tabular and folded Albian strata that are overlain by thin (<1 cm) post-Albian growth strata (Figure 11). These folds are formed by salt and overburden basinward translation and consequent downdip shortening by buttressing of salt flow against landward-dipping base-salt steps.

5 | DISCUSSION

5.1 | Understanding salt tectonic processes in the Santos Basin

Our experiment simulated three-dimensionally variable salt flow and overburden deformation across a complex set of base-salt structures; by doing this, our model explored the origin and evolution of salt-tectonics structures imaged in seismic reflection data in the southern Santos Basin, offshore Brazil (Figures 2–4). The base-salt geometry in the model reproduces the observed regional structural framework (Figures 3 and 4) (cf. Pichel, Jackson, et al., 2019; Pichel et al., 2021; Rodriguez et al., 2019), which is defined by a regionally basinward-dipping base-salt, and a large proximal half-graben (the Merluza Graben) that passes downdip onto a set of landward-dipping base-salt steps that form the edge of the SPP (Figures 3, 4 and 9–11). Our model also reproduces the main structural styles and related kinematics inferred from recent seismic reflection-based studies, supporting the view that the key salt-tectonic processes operating in the basin were post-salt gravity-driven gliding and spreading over three-dimensionally variable base-salt topography (Pichel et al., 2021; Pichel, Finch, et al., 2019; Pichel, Jackson, et al., 2019; Pichel & Jackson, 2020). Our experiments are thus suitable to test these recent hypotheses regarding the origin of the specific salt-tectonic structural styles present within the basin, and those identified in similar salt-influenced settings.

Our model displays similar distribution, size and geometries of salt (i.e., diapirs, rollers and inflated salt plateaus) and post-salt structures (i.e., rafts, rollovers and minibasins) to the study area (Figures 3 and 11–13). It also shows similar evolution and kinematics to what has been proposed by recent studies (Pichel et al., 2021; Pichel & Jackson, 2020). For example, salt rollers and extensional

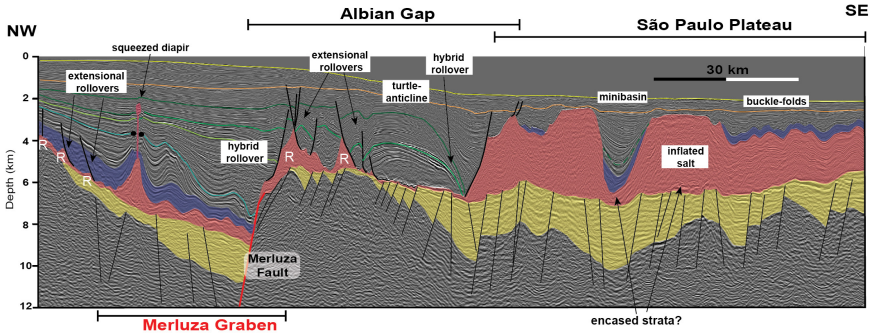

FIGURE 12 Regional seismic profile from the southern Santos Basin illustrating its main rift and salt-related structural provinces, the sub-salt Merluza graben, which passes downdip and partially overlaps laterally with the supra-salt Albian Gap and the inflated salt diapirs and salt-cored folds in the São Paulo Plateau. Base-, top-salt and supra-salt structures are markedly similar to regional model cross-sections shown in Figure 9.

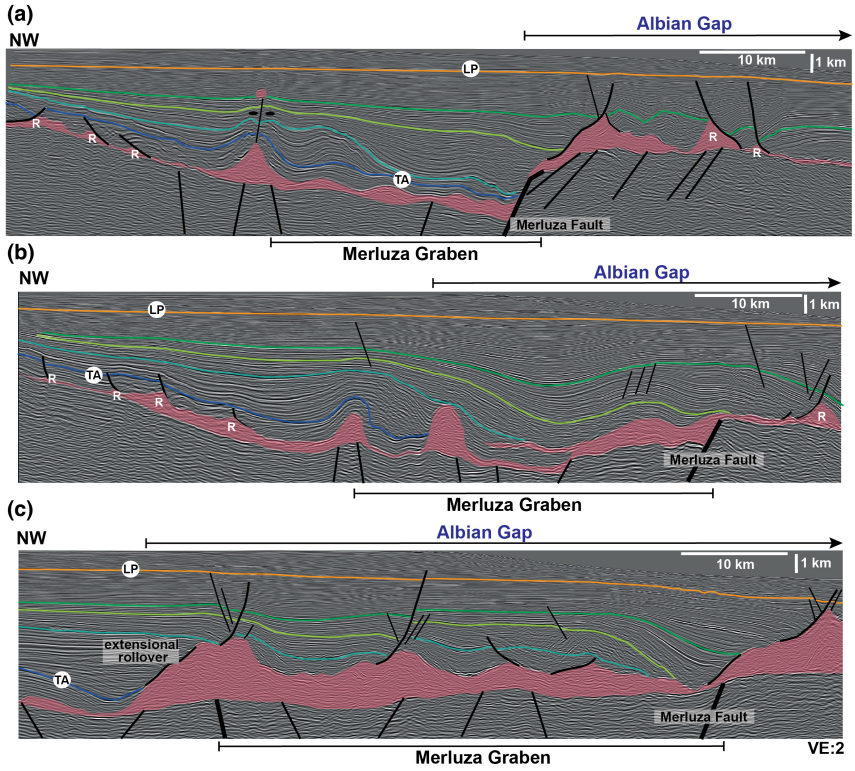

FIGURE 13 Seismic profiles from the (a,b) north domain and (c) south domain of the study-area in the southern Santos basin, showing similar styles, spatial and temporal distribution of salt and supra-salt structures and their relationship to base-salt topography associated with the Merluza graben and the Merluza fault to our model. In (a), salt rollers and extensional rollovers pass downdip to a squeezed diapir over the Merluza graben, an extensional basinward-dipping supra-salt rollover above the Merluza fault and large salt rollers with landward-dipping extensional rollovers at its footwall crest. In (b), there are similar styles of structures with the main difference being above the Merluza fault, whereas instead of an extensional rollover there is an inflated salt structure with a landward-verging salt-wing over the Merluza fault and overlain by an expulsion-dominated rollover. In (c), where the Merluza graben is oblique and wider, deformation is characterized by inflated salt directly overlain by post-Albian rollover strata and normal faults showing extensional reactivation of previously inflated salt.

rollovers form in the updip portion of the Merluza Graben, and complex, multiphase diapirs form adjacent to the Merluza Fault due to early salt inflation followed by late salt expulsion and overburden extension (Figures 5–13). Post-Albian rollovers and turtle anticlines form adjacent to and downdip of the Merluza Fault, directly overlying depleted salt (i.e., Albian strata are absent; Figures 7–13). The modelled Albian Gap presents nearly identical dimensions, geometry (i.e., depleted salt, turtle anticlines and variable types of rollovers) and relationship to the underlying pre-salt framework to the south-central portion of the Albian Gap in nature

(Figures 6–13). The Albian Gap extends laterally beyond the Merluza Graben but where they both intersect the Albian Gap is wider (>50 km) and more structurally variable (Figures 3, 12 and 13). The Merluza Graben played thus a crucial role on the dimensions and complexity of the Albian Gap by (i) creating greater salt flux variations over its greater base-salt relief, and (ii) by favouring the development of a larger precursor diapir relative to its central-northern domains where the Albian Gap is narrower (<40 km) and more extension-dominated (cf. Pichel & Jackson, 2020; Rowan et al., 2022). In the SPP, there is salt inflation and development of broad diapirs and salt-cored buckle-folds (Figure 10) (cf. Pichel et al., 2018; Pichel, Jackson, et al., 2019). The arrangement of these features indicates an alternation in time and space between load-driven diapirism, driven primarily by spreading, and overburden extension, driven by a combination between gliding and spreading.

Although successfully reproducing many of the key salt and overburden structures, and the kinematics inferred to lead to their development, there are discrepancies between our model and what we observe in nature. For example, in our model, especially within the analogue Merluza Graben, there is: (i) a greater occurrence of turtle anticlines in its updip portion, (ii) a greater complexity and number of diapirs and (iii) less salt near or above the Merluza Fault, where there are larger primary welds (Figures 9–11). We also note that in our model, throw does not vary along strike of the Merluza Fault, whereas it decreases southwards in nature (Figure 13). These discrepancies may be related to parameters that were not modelled here such as (i) salt stratigraphy/internal mechanics, and/or, (ii) variation of the post-salt sedimentation rates and, in particular, (iii) post-salt reactivation of sub-salt normal faults (Pichel et al., 2021), all of which are worthy of testing in future studies. Post-salt reactivation of sub-salt faults would imply an originally thinner salt and a gentler basinward dip of the base-salt within the graben at the time of salt deposition. This would inhibit gliding and diapirism in its updip portion and could explain, at least partially, these discrepancies. In addition, the reactivation of sub-salt faults by thick-skinned extension would likely promote less salt extrusion within and basinward of the half-graben by moving both base- and top-salt downwards and, consequently, halt the development of complex diapir geometries. It would also favour more salt flow towards and being trapped against its main fault, explaining why in our models, where the salt layer is not disrupted, the salt deposited over the modelled Merluza Fault is able to flow basinward of this structure.

We also observe in our models Albian-equivalent strata encased within the salt, above the distal sub-salt plateau (Figure 6a,b). These features form due to basinward advance of the near-surface salt walls over previously folded pre-kinematic post-salt strata (Figure 6a,b). Although such structures have not yet been described from the Santos Basin, they have been observed in other salt basins (e.g., Precaspian, Fernandez et al., 2017) and other physical models (Brun & Fort, 2011). These structures could have formed as a limitation of our modelling approach associated with the lack of pelagic-type sedimentation in the deep-basin, which could have impeded basinward translation of the salt plateau and consequent encasement of the folded post-salt strata. However, it is also possible that these features *do* occur in the Santos Basin but have not yet been properly imaged or drilled. The presence of seismically reflective, disrupted and folded strata within some salt walls in the SPP (Figure 12), like the ones observed in our models (Figures 9–11), may support this hypothesis.

5.2 | The interplay between three-dimensionally variable base-salt relief, gliding and spreading

Our 3D physical experiments capture the complex evolution of gravity-driven salt tectonics in response to the interplay between gliding and spreading across complex base-salt relief. Our work expands on the recent advances in our understanding of the dynamics of salt flow over base-salt relief (cf., Dooley et al., 2017, 2018; Ferrer et al., 2017; Pichel, Finch, et al., 2019) by: (i) simulating salt flow over more variable base-salt geometries then previously considered (i.e., base-salt steps oblique and not simply orthogonal to salt-detached tectonic transport); and (ii) by exploring the interplay between progradation- and sediment load-induced spreading *and* gravity gliding (Figure 14).

In our experiments, the landward-dipping sub-salt normal faults produce semi-isolated salt sub-basins that promote strong partitioning of salt flow and overburden translation. Salt flows basinward along basinward-dipping hangingwalls before it is buttressed against the landward-dipping faults (Figure 14). This generates extension with the development of fault-bounded salt rollers, extensional turtles and/or rollovers and down-dip salt inflation and shortening over their bounding landward-dipping faults and/or their footwall crests (Figures 5a and 14a,b). These sub-salt faults correspond to the sites of diapir nucleation, with these structures subsequently translated away from the place where they originally formed. This style of structural partition has been observed in previous physical analogue models (cf., Dooley et al., 2017, 2018; Dooley & Hudec, 2017; Pichel, Finch, et al., 2019).

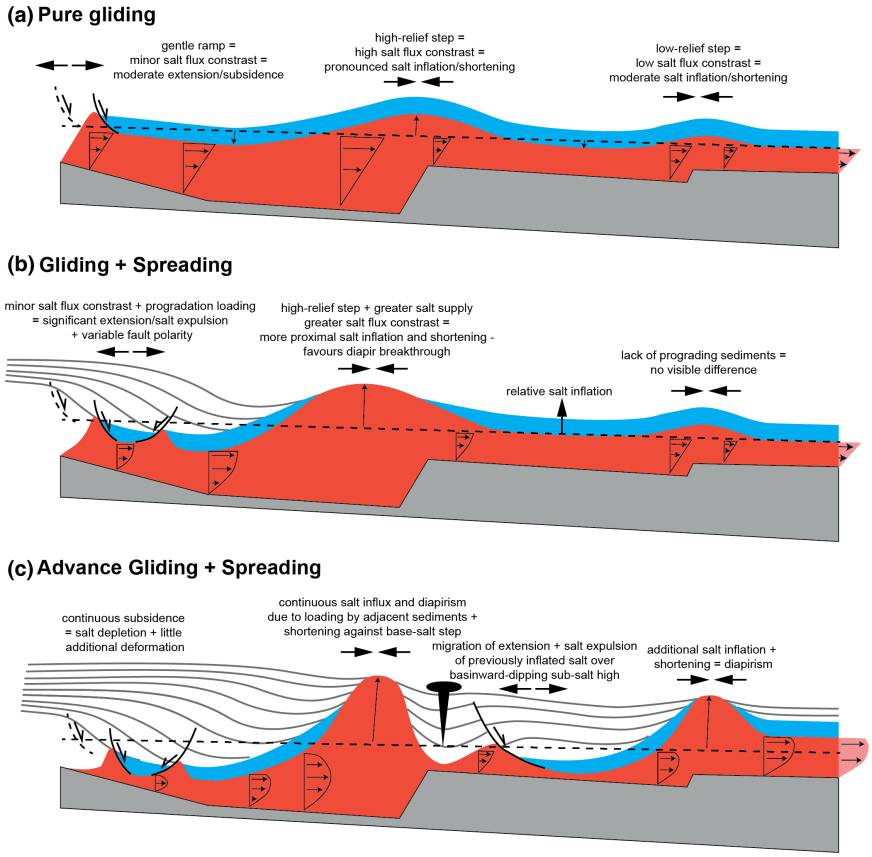

FIGURE 14 (a) Synthetic diagram illustrating the effects of gliding over asymmetric base-salt relief based on experiments from Dooley et al. (2017, 2018). In (b) and (c), synthetic diagrams showing the interplay between gliding and spreading associated with prograding sedimentary wedges over the same base-salt relief as simulated in our models and observed in the southern Santos Basin. In the initial stages, where prograding sediments are focused within the most proximal graben there is updip extension in the form of salt rollers and extensional rollovers above the basinward-dipping hangingwall and significant salt inflation and diapirism against its fault. This is similar to the simpler gliding scenario shown in (a), although the degree of updip extension and salt evacuation, as well as of basinward salt inflation is amplified by the differential sedimentary loading and results in larger and likely more diapiric salt structures. With continued progradation (c), sediments reach the downdip sub-salt high and the area that was previously located ahead of the progradation front and characterized by salt inflation. This results in salt evacuation and extension of previously inflated salt over sub-salt high and additional inflation further downdip.

Our experiment also shows that differential loading can either enhance or reduce the effects of typical salt flux variations driven by gliding over base-salt relief, depending on where the prograding slope lies relative to the base-salt relief (Figure 14c). This influences the spatial and temporal distribution of salt structures (Figure 14b,c). For example, progradation and differential loading over basinward-dipping hangingwalls can amplify top-salt subsidence over the hangingwalls and consequently salt inflation against their bounding landward-dipping faults. This favours the development of diapirs and associated minibasins and/or expulsion rollovers that are larger than in a pure gliding scenario (Figure 14a,b). This is observed over the Merluza Fault in the Santos Basin (Figures 12 and 13) and the equivalent structure in our experiment (Figures 5–11), which have diapir and minibasin geometries larger than the ones reproduced in analogue models with minimal influence of spreading (cf. Dooley et al., 2017, their Figure 14a).

Conversely, salt expulsion from underneath prograding sediments may promote transient salt inflation and shortening above basinward-dipping hangingwalls, where extension would be expected if deformation was driven primarily by gliding. This is the case when basinward-dipping base-salt segments lie immediately basinward of the prograding wedge (Figures 5 and 14b). This is observed in our model where early salt inflation and contraction (i.e., buckle-folding) occurred ahead of the progradational front and above the basinward-dipping footwall of the largest pre-salt fault, that is, Merluza Fault (Figures 5, 8a,b, 14a,b). As the sediment wedge progrades and the locus of maximum load shifts basinward, beyond the fault, the initially inflated salt and contractional domain extends (Figures 6, 8c,d, 14c). This is observed in

both model and natural examples by the relatively late development of fault-bounded salt rollers and extensional and/or hybrid (extension-expulsion) rollovers and turtle anticlines, above previously inflated salt in the footwall of the Merluza Fault (Figures 6–13).

The timing, geometry and distribution of the salt structures are also influenced by the orientation (i.e., obliquity) of sub-salt faults and related half-grabens relative to the direction of tectonic transport, which in turn controls also the steepness of base-salt steps (Figures 9–11). Consequently, the orientations and dimensions of salt and overburden structures change between the northern and southern domains of our model (Figures 5–6) and in nature (Figure 3), as they tend to follow the trend of the base-salt topography. For example, these structures are perpendicular to the direction of tectonic transport in the northern domain and oblique in the southern domain (Figures 3 and 5–6). In the northern domain, the largest pre-salt graben is narrower and orthogonal to the tectonic transport, promoting greater salt inflation and overburden uplift, which is aided by (simulated) erosion, and that promotes earlier (i.e., Albian) development of a large diapir (Figure 5a,b). In the south domain, the wider and oblique pre-salt graben produces an equally wide, inflated salt structure. In both domains, the inflated salt has a broadly similar planform to the underlying graben (Figure 5). Because of its greater width and the obliquity of base-salt relief, salt inflation and overburden uplift are less pronounced, albeit distributed over a wider area than in the north domain. For that reason, the salt is not able to breakthrough to form a diapir in the southern domain; this can only occur in the northern domain (Figure 5). In the north, the diapir can advance earlier and faster beyond its sub-salt bounding fault, thus becoming gradually wider than laterally equivalent salt structures in the south (Figures 5 and 6).

These lateral variations of salt flow produce gradients of salt supply and overburden thickness throughout the remaining model evolution. This results in contrasting styles, kinematics and dimension of salt structures between the northern and southern domains (Figures 5–9). In the north, where the graben was narrower, there was greater and earlier salt expulsion from the graben onto the adjacent base-salt plateau. This resulted in greater salt and overburden translation and consequently, a greater occurrence of fault-bounded salt rollers and basinward-dipping normal faults in the footwall of the Merluza Fault (Figures 6–13). In the south, less salt was expelled from the Merluza Graben onto the base-salt plateau, resulting in an initially smaller salt supply and consequently less salt and overburden translation in the footwall of the Merluza Fault. Thus, more salt remained there towards the end of the model, producing taller and more symmetric, load-driven diapirs and minibasins (Figures 9–11). This also meant less seaward salt inflation above the base-salt plateau in the southern domain than in the northern domain (Figures 6–11). This spatial and temporal variability of salt deformation is also observed by variations in flow vectors in overhead DIC images (Figure 7). Where base-salt structures are oblique to transport, there is generally a change in the direction and magnitude of salt flow. For example, in the early stage of model evolution, there is divergent salt flow where the Merluza Fault is oblique to the transport direction, with salt flow also becoming oblique to the main direction of tectonic transport (Figure 7a,b). At the early stages of model evolution, the magnitude of lateral salt flow is also greater in the south, within the oblique portion of the Merluza Graben where the landward-dipping base-salt step is gentler (Figure 7a,b). Conversely, vertical salt flow and inflation are greater in the north where the sub-salt graben and its bounding fault are orthogonal to the transport direction (Figure 7a,b). These earlier patterns, however, change at later stages as salt breaks through the cover to form passive diapirs that accommodate greater lateral salt flow, widening and/or translating faster than areas covered by sediments (Figure 7b–d). This is seen at intermediate model stages (Figures 6 and 7b,c), as lateral salt flow is greater in the north, along the wide diapir formed above the orthogonal segment of the Merluza Fault.

5.3 | Gravity-driven fault polarity and rollover kinematics

Another important feature observed in our model is the spatial and temporal variability between normal fault polarity, extension-, and expulsion-related processes and their resulting depocenter geometries (i.e., rollover, minibasins and turtles) (Figures 9–11). For each basinward-dipping base-salt segment, there is commonly a transition between proximal and/or earlier basinward-dipping faults transitioning downdip, and through time, into landward-dipping faults (Figure 9). This suggests that basinward-dipping normal faults tend to form earlier when the overburden is thinner and thus, primarily by gliding, whereas landward-dipping (i.e., counter-regional) faults form later when differential loading (i.e., spreading) becomes more dominant. Counter-regional normal faults also seem to be favoured over relatively thicker or inflated salt as opposed to initially thinner and/or welded salt for basinward-dipping normal faults (cf., Dooley et al., 2018). Whereas basinward-dipping normal faults are readily associated with extensional rollover geometries, the landward-dipping faults also

have more variable growth strata (i.e., rollover and/or upturned halokinetic-sequences) throughout their width and height (Figures 9–11).

Extension rollovers are characterized by stratal thickening and downturn towards normal faults (cf. Jackson & Hudec, 2017). In contrast, expulsion rollovers are defined by sigmoidal growth strata that thicken seaward, before thinning towards and being upturned against their bounding structure, which can be a salt diapir or anticline, and/or normal faults (cf., Jackson & Hudec, 2017; Pichel & Jackson, 2020). These are end-member geometries, and it is likely that a combination and/or alternation of these two processes occur in nature. We thus follow Pichel and Jackson (2020) and use the term extension- and expulsion-dominated rollovers to describe these end-member styles and, in the case where both processes have a broadly similar contribution, hybrid-rollovers. In our model, extension-dominated rollovers and related turtles are observed almost exclusively in the most proximal part of the model, updip and above the hangingwall of the Merluza Fault, where the base-salt dips basinward and where salt was originally thinner (Figures 9–11). Further seaward, adjacent to and beyond the Merluza Fault, there are expulsion-dominated rollovers that are characterized by basinward-dipping sigmoidal growth strata locally upturned against inflated salt diapirs (Figures 9–11). These occur above either basinward-dipping (Figures 9a and 10a) or landward-dipping base-salt domains (Figures 10b and 11a), forming preferentially in areas of previously inflated salt (Figures 5 and 6). Hybrid rollovers occur between those two areas, that is, between the extension-dominated and expulsion-dominated rollovers, above and updip of the Merluza Fault (Figures 10 and 11a). These geometries and spatial distribution relative to the Merluza Fault are also observed in nature (Figures 12 and 13).

5.4 | Limitations and future work

As with all models, this one also presents obvious limitations. There are other parameters that despite having only local or second-order importance in the study area and, thus are not included in this model, may be important in other salt basins. For example, our model does not include reactivation of pre-salt normal faults coeval to gravity-driven salt tectonics. This is likely to have occurred in portions of the Campos-Santos basins (cf., Davison et al., 2012; Pichel et al., 2021) as well as other salt-bearing rifted margins, such as northern Gulf of Mexico, West Africa and the North, Red and Barents seas. These locations are also characterized by different rift-related base-salt geometries (i.e., half-grabens with different fault polarities) that despite not being as important in the study area as the ones modelled here, are relevant for other parts of Santos (e.g., seaward of the SPP) and other salt basins. These and other parameters such as (i) different post-salt sedimentation rates, and (ii) variable along-strike sub-salt fault throw have not been included in this experiment and are thus worthy of future testing using either physical or numerical models.

6 | CONCLUSIONS

Our model simulates three-dimensionally variable salt flow driven by the interplay between gravity-gliding and spreading over laterally variable base-salt relief to test recent hypotheses (cf., Pichel & Jackson, 2020; Pichel et al., 2021) for the kinematics of salt tectonics in the controversial Santos Basin. The model produces a remarkably similar evolution and architecture of salt and post-salt deformation to the study-area and offers an improved understanding on the interaction and distribution of salt-related gravity-driven processes and their resultant structural styles. They illustrate the primary controls on the genesis and 3D variability of depocentres (i.e., extension- vs. expulsion-dominated rollovers, turtle anticlines vs. minibasins), normal faults (i.e., counter-regional vs. regional faults) and salt structures (i.e., reactive vs. passive diapirs). Basinward-dipping faults tend to form earlier when the overburden is thinner and driven primarily by gliding, whereas landward-dipping faults form later when differential loading (i.e., spreading) becomes more dominant and/or above thickened or inflated salt. Basinward-dipping faults are readily associated with extensional rollover geometries whereas landward-dipping faults present more variable growth strata (i.e., rollover and/or upturned halokinetic-sequences). The model also sheds light on the lateral variability of salt and overburden translation owing to laterally variable base-salt relief and the dynamically evolving salt supply, such as the effects of oblique versus orthogonal, and steep versus gentle base-salt relief on the orientation, dimension and styles of salt structures. This explains, for example, the initiation of a ca. 30 km wide near-surface diapir precursor of the Albian Gap by gliding and spreading over a pronounced and orthogonal base-salt step associated with the Merluza Fault, something not previously modelled. The structural processes and salt-related geometries modelled are also comparable and relevant to many other salt-bearing rifted margins (e.g., Gulf of Mexico, West Africa, Nova Scotia and other parts of Brazil).

ACKNOWLEDGEMENTS

We would like to thank Imperial College London for awarding the Arthur Holmes Centenary Grant which covered all travelling expenses of the first author to work for 1 month at the Geomodels Analogue Modelling Laboratory, Universitat de Barcelona. The study has also been supported by the research project Structure and Deformation of Salt-bearing Rifted Margins (SABREM) (PID 2020-117598GB-I00) funded by MCIN/AEI/10.13039/501100011033. We thank Ian Davison, Tim Dooley, Sian Evans and an anonymous reviewer for the detailed and constructive reviews. We also thank Rachelle Kernen (AAPG bulletin) and Zoe Mildon (Basin Research) for their excellent and constructive editorial handling. We thank Frank Peel for the insightful discussions about tectonics in the Santos Basin. We thank Oscar Gratacos and Marco Snidero for helping to flip the enormous model used in this study.

DATA AVAILABILITY STATEMENT

The data that support the findings of this study are available on request from the corresponding author. The data are not publicly available due to privacy or ethical restrictions.

ORCID

Leonardo M. Pichel https://orcid.org/0000-0001-8692-3831
Oriol Ferrer https://orcid.org/0000-0001-5545-9992
Christopher A.-L. Jackson https://orcid.org/0000-0002-8592-9032
Eduard Roca https://orcid.org/0000-0002-0827-4175

REFERENCES

Adam, J., & Krézsek, C. (2012). Basin-scale salt tectonic processes of the Laurentian Basin, eastern Canada: Insights from integrated regional 2D seismic interpretation and 4D physical experiments. *Geological Society, London, Special Publications*, *363*(1), 331–360.

Adam, J., Urai, J., Wieneke, B., Oncken, O., Pfeiffer, K., Kukowski, N., Lohrmann, J., Hoth, S., van der Zee, W., & Schmatz, J. (2005). Shear localisation and strain distribution during tectonic faulting—New insights from granular-flow experiments and high-resolution optical image correlation techniques. *Journal of Structural Geology*, *27*, 283–301. https://doi.org/10.1016/j.jsg.2004.08.008

Brun, J. P., & Fort, X. (2011). Salt tectonics at passive margins: Geology versus models. *Marine and Petroleum Geology*, *28*(6), 1123–1145.

Cobbold, P. R., Szatmari, P., Demercian, L. S., Coelho, D., & Rossello, E. A. (1995). Seismic and experimental evidence for thin-skinned horizontal shortening by convergent radial gliding on evaporites, deep-water Santos Basin, Brazil. In M. P. A. Jackson, D. G. Roberts, & S. Snelson (Eds.), *Salt tectonics: A global perspective* (Vol. *65*, pp. 305–321). AAPG Memoir.

Davison, I., Anderson, L., & Nuttall, P. (2012). Salt deposition, loading and gravity drainage in the Campos and Santos salt basins. *Geological Society of London Special Publications*, *363*(1), 159–174.

Dell'Ertole, D., & Schellart, W. P. (2013). The development of sheath folds in viscously stratified materials in simple shear conditions: An analogue approach. *Journal of Structural Geology*, *56*, 129–141. https://doi.org/10.1016/j.jsg.2013.09.002

Demercian, S., Szatmari, P., & Cobbold, P. R. (1993). Style and pattern of salt diapirs due to thin-skinned gravitational gliding, Campos and Santos basins, offshore Brazil. *Tectonophysics*, *228*(3–4), 393–433.

Deptuck, M. E., & Kendell, K. L. (2017). A review of Mesozoic-Cenozoic salt tectonics along the Scotian margin, eastern Canada. In J. I. Soto, J. Flinch, & G. Tari (Eds.), *Permo-Triassic Salt Provinces of Europe, North Africa and the Atlantic Margins: Tectonics and Hydrocarbon Potential* (pp. 287–312). Elsevier. https://doi.org/10.1016/B978-0-12-809417-4.00014-8

do Amarante, F. B., Jackson, C. A. L., Pichel, L. M., dos Santos Scherer, C. M., & Kuchle, J. (2021). Pre-salt rift morphology controls salt tectonics in the Campos Basin, offshore SE Brazil. *Basin Research*, *33*(5), 2837–2861.

Dooley, T. P., & Hudec, M. R. (2017). The effects of base-salt relief on salt flow and suprasalt deformation patterns — Part 2: Application to the eastern Gulf of Mexico. *Interpretation*, *5*(1), SD25–SD38.

Dooley, T. P., Hudec, M. R., Carruthers, D., Jackson, M. P., & Luo, G. (2017). The effects of base-salt relief on salt flow and suprasalt deformation patterns—Part 1: Flow across simple steps in the base of salt. *Interpretation*, *5*(1), SD1–SD23.

Dooley, T. P., Hudec, M. R., Pichel, L. M., & Jackson, M. P. (2018). The impact of base-salt relief on salt flow and suprasalt deformation patterns at the autochthonous, paraautochthonous and allochthonous level: Insights from physical models. *Geological Society, London, Special Publications*, *476*, 287–315.

Dooley, T. P., Jackson, M. P., & Hudec, M. R. (2007). Initiation and growth of salt-based thrust belts on passive margins: Results from physical models. *Basin Research*, *19*(1), 165–177.

Evans, S. L., & Jackson, C. A. L. (2020). Base-salt relief controls salt-related deformation in the outer Kwanza Basin, offshore Angola. *Basin Research*, *32*(4), 668–687.

Fernandez, N., Duffy, O. B., Hudec, M. R., Jackson, M. P., Burg, G., Jackson, C. A. L., & Dooley, T. P. (2017). The origin of salt-encased sediment packages: Observations from the SE Precaspian Basin (Kazakhstan). *Journal of Structural Geology*, *97*, 237–256.

Ferrer, O., Gratacos, O., Roca, E., & Munoz, J. A. (2017). Modeling the interaction between presalt seamounts and gravitational failure in salt-bearing passive margins: The Messinian case in the northwestern Mediterranean Basin. *Interpretation*, *5*, 99–117.

Fiduk, J. C., & Rowan, M. G. (2012). Analysis of folding and deformation within layered evaporites in blocks BM-S-8 & -9, Santos Basin, Brazil. *Geological Society, London, Special Publications*, *363*(1), 471–487.

Garcia, S. F., Letouzey, J., Rudkiewicz, J. L., Danderfer Filho, A., & de Lamotte, D. F. (2012). Structural modeling based on sequential restoration of gravitational salt deformation in the Santos Basin (Brazil). *Marine and Petroleum Geology*, *35*(1), 337–353.

Ge, H., Jackson, M. P., & Vendeville, B. C. (1997). Kinematics and dynamics of salt tectonics driven by progradation. *AAPG Bulletin*, *81*(3), 398–423.

Gemmer, L., Ings, S. J., Medvedev, S., & Beaumont, C. (2004). Salt tectonics driven by differential sediment loading: Stability analysis and finite-element experiments. *Basin Research*, *16*(2), 199–218.

Gemmer, L., Beaumont, C., & Ings, S. J. (2005). Dynamic modelling of passive margin salt tectonics: Effects of water loading, sediment properties and sedimentation patterns. *Basin Research*, *17*(3), 383–402.

Giles, K. A., & Rowan, M. G. (2012). Concepts in halokinetic-sequence deformation and stratigraphy. *Geological Society, London, Special Publications*, *363*(1), 7–31.

Gomes, P. O., Kilsdonk, B., Minken, J., Grow, T., & Barragan, R. (2009). The outer high of the Santos Basin, southern São Paulo plateau, Brazil: Pre-salt exploration outbreak, paleogeographic setting, and evolution of the syn-rift structures. In *AAPG International Conference and Exhibition* (pp. 15–18).

Guerra, M. C., & Underhill, J. R. (2012). Role of halokinesis in controlling structural styles and sediment dispersal in the Santos Basin, offshore Brazil. *Geological Society, London, Special Publications*, *363*(1), 175–206.

Heine, C., Zoethout, J., & Müller, R. D. (2013). Kinematics of the South Atlantic rift. *Solid Earth*, *4*(2), 215–253.

Horsfield, W. T. (1977). An experimental approach to basement-controlled faulting. *Geologie en Mijnbouw*, *56*, 363–370.

Hubbert, M. K. (1951). Mechanical basis for certain familiar geologic structures. *Geological Society of America Bulletin*, *62*(2), 355.

Hudec, M. R., Dooley, T. P., Peel, F. J., & Soto, J. I. (2020). Controls on the evolution of passive-margin salt basins: Structure and evolution of the Salina del bravo region, northeastern Mexico. *Bulletin*, *132*(5–6), 997–1012.

Jackson, C. A. L., Rodriguez, C. R., Rotevatn, A., & Bell, R. E. (2014). Geological and geophysical expression of a primary salt weld: An example from the Santos Basin, Brazil. *Interpretation*, *2*(4), SM77–SM89.

Jackson, C. A. L., Jackson, M. P., & Hudec, M. R. (2015). Understanding the kinematics of salt-bearing passive margins: A critical test of competing hypotheses for the origin of the Albian gap, Santos Basin, offshore Brazil. *Geological Society of America Bulletin*, *127*(11–12), 1730–1751.

Jackson, C. A. L., Jackson, M. P., Hudec, M. R., & Rodriguez, C. R. (2015). Enigmatic structures within salt walls of the Santos Basin—Part 1: Geometry and kinematics from 3D seismic reflection and well data. *Journal of Structural Geology*, *75*, 135–162.

Jackson, M. P., & Hudec, M. R. (2017). *Salt tectonics: Principles and practice*. Cambridge University Press.

Karner, G. D., & Gambôa, L. A. P. (2007). Timing and origin of the South Atlantic pre-salt sag basins and their capping evaporites. *Geological Society, London, Special Publications*, *285*(1), 15–35.

Krézsek, C., Adam, J., & Grujic, D. (2007). Mechanics of fault and expulsion rollover systems developed on passive margins detached on salt: Insights from analogue modelling and optical strain monitoring. *Geological Society, London, Special Publications*, *292*(1), 103–121.

Kukla, P. A., Strozyk, F., & Mohriak, W. U. (2018). South Atlantic salt basins—Witnesses of complex passive margin evolution. *Gondwana Research*, *53*, 41–57.

Lebit, H., Arasanipalai, S., Tilton, J., & Ollagnon, P. (2019). *Santos vision: Innovative seismic data processing in a super giant oil basin*. GeoExPro.

Magee, C., Pichel, L. M., Madden-Nadeau, A. L., Jackson, C. A. L., & Mohriak, W. (2020). Salt-magma interactions influence intrusion distribution and salt tectonics in the Santos Basin, offshore Brazil. *Basin Research*, *33*(3), 1820–1843.

Meisling, K. E., Cobbold, P. R., & Mount, V. S. (2001). Segmentation of an obliquely rifted margin, Campos and Santos basins, southeastern Brazil. *AAPG Bulletin*, *85*(11), 1903–1924.

Modica, C. J., & Brush, E. R. (2004). Postrift sequence stratigraphy, paleogeography, and fill history of the deep-water Santos Basin, offshore Southeast Brazil. *AAPG Bulletin*, *88*(7), 923–945.

Mohriak, W. U., Macedo, J. M., Castellani, R. T., Rangel, H. D., Barros, A. Z. N., Latgé, M. A. L., Mizusaki, A. M. P., Szatmari, P., Demercian, L. S., Rizzo, J. G., & Aires, J. R. (1995). Salt tectonics and structural styles in the deep-water province of the Cabo Frio region, Rio de Janeiro, Brazil. In M. P. A. Jackson, D. G. Roberts, & S. Snelson (Eds.), *Salt tectonics: A global perspective* (Vol. *65*, pp. 273–304). AAPG Memoir.

Mohriak, W., Nemčok, M., & Enciso, G. (2008). South Atlantic divergent margin evolution: Rift-border uplift and salt tectonics in the basins of SE Brazil. *Geological Society, London, Special Publications*, *294*(1), 365–398.

Pichel, L. M., Peel, F., Jackson, C. A.-L., & Huuse, M. (2018). Geometry and kinematics of salt-detached ramp syncline basins. *Journal of Structural Geology*, *115*, 208–230. https://doi.org/10.1016/j.jsg.2018.07.016

Pichel, L. M., Huuse, M., Redfern, J., & Finch, E. (2019). The influence of base-salt relief, rift topography and regional events on salt tectonics offshore Morocco. *Marine and Petroleum Geology*, *103*, 87–113.

Pichel, L. M., Finch, E., & Gawthorpe, R. L. (2019). The impact of pre-salt rift topography on salt tectonics: A discrete-element modeling approach. *Tectonics*, *38*(4), 1466–1488.

Pichel, L. M., Jackson, C. A. L., Peel, F., & Dooley, T. P. (2019). *Base-salt relief controls salt-tectonic structural style, São Paulo plateau, Santos Basin, Brazil*. Basin Research.

Pichel, L. M., & Jackson, C. A. L. (2020). The enigma of the Albian gap: Spatial variability and the competition between salt expulsion and extension. *Journal of the Geological Society*, *177*(6), 1129–1148.

Pichel, L. M., Jackson, C. A. L., Peel, F., & Ferrer, O. (2021). The Merluza Graben: How a failed spreading center influenced margin structure, and salt deposition and tectonics in the Santos Basin. *Brazil. Tectonics*, *40*(10), e2020TC006640.

Quirk, D. G., Schødt, N., Lassen, B., Ings, S. J., Hsu, D., Hirsch, K. K., & Von Nicolai, C. (2012). Salt tectonics on passive margins: Examples from Santos, Campos and kwanza basins. *Geological Society, London, Special Publications*, *363*(1), 207–244.

Rodriguez, C. R., Jackson, C. L., Rotevatn, A., Bell, R. E., & Francis, M. (2019). Dual tectonic-climatic controls on salt giant deposition in the Santos Basin, offshore Brazil. *Geosphere*, *14*(1), 215–242.

Rowan, M. G., & Ratliff, R. A. (2012). Cross-section restoration of salt-related deformation: Best practices and potential pitfalls. *Journal of Structural Geology*, *41*, 24–37.

Rowan, M. G., Tilton, J., Lebit, H., & Fiduk, J. C. (2022). Thin-skinned extensional salt tectonics, counterregional faults, and

the Albian gap of Brazil. *Marine and Petroleum Geology*, *137*, 105478.

Tari, G., & Jabour, H. (2013). Salt tectonics along the Atlantic margin of Morocco. *Geological Society, London, Special Publications*, *369*(1), 337–353.

Weijermars, R., & Schmeling, H. (1986). Scaling of Newtonian and non-Newtonian fluid dynamics without inertia for quantitative modelling of rock flow due to gravity (including the concept of rheological similarity). *Physics of the Earth and Planetary Interiors*, *43*, 316–330.

How to cite this article: Pichel, L. M., Ferrer, O., Jackson, C-L., & Roca, E. (2022). Physical modelling of the interplay between salt-detached gravity gliding and spreading across complex rift topography, Santos Basin, offshore Brazil. *Basin Research*, *00*, 1–22. https://doi.org/10.1111/bre.12695